



Exonic Splicing Mutations Are More Prevalent than Currently Estimated and Can Be Predicted by Using In Silico Tools

Omar Soukarieh, Pascaline Gaildrat, Mohamad Hamieh, Aurélie Drouet, Stéphanie Baert-Desurmont, Thierry Frébourg, Mario Tosi, Alexandra Martins

► To cite this version:

Omar Soukarieh, Pascaline Gaildrat, Mohamad Hamieh, Aurélie Drouet, Stéphanie Baert-Desurmont, et al.. Exonic Splicing Mutations Are More Prevalent than Currently Estimated and Can Be Predicted by Using In Silico Tools. PLoS Genetics, 2016, 12 (1), pp.e1005756. 10.1371/journal.pgen.1005756 . inserm-02160189

HAL Id: inserm-02160189

<https://inserm.hal.science/inserm-02160189>

Submitted on 19 Jun 2019

HAL is a multi-disciplinary open access archive for the deposit and dissemination of scientific research documents, whether they are published or not. The documents may come from teaching and research institutions in France or abroad, or from public or private research centers.

L'archive ouverte pluridisciplinaire **HAL**, est destinée au dépôt et à la diffusion de documents scientifiques de niveau recherche, publiés ou non, émanant des établissements d'enseignement et de recherche français ou étrangers, des laboratoires publics ou privés.

RESEARCH ARTICLE

Exonic Splicing Mutations Are More Prevalent than Currently Estimated and Can Be Predicted by Using *In Silico* Tools

Omar Soukarieh¹, Pascaline Gaildrat¹, Mohamad Hamieh^{1*}, Aurélie Drouet¹, Stéphanie Baert-Desurmont^{1,2}, Thierry Frébourg^{1,2}, Mario Tosi¹, Alexandra Martins^{1*}

1 Inserm U1079-IRIB, University of Rouen, Normandy Centre for Genomic and Personalized Medicine, Rouen, France, **2** Department of Genetics, University Hospital, Normandy Centre for Genomic and Personalized Medicine, Rouen, France

✉ Current Address: The Center for Cell Engineering, Memorial Sloan Kettering Cancer Center; Immunology Program, Sloan Kettering Institute, Memorial Sloan Kettering Cancer Center, New York, New York, United States of America

* alexandra.martins@univ-rouen.fr



OPEN ACCESS

Citation: Soukarieh O, Gaildrat P, Hamieh M, Drouet A, Baert-Desurmont S, Frébourg T, et al. (2016) Exonic Splicing Mutations Are More Prevalent than Currently Estimated and Can Be Predicted by Using *In Silico* Tools. PLoS Genet 12(1): e1005756. doi:10.1371/journal.pgen.1005756

Editor: Stefan Aretz, University Hospital Bonn, GERMANY

Received: July 26, 2015

Accepted: December 1, 2015

Published: January 13, 2016

Copyright: © 2016 Soukarieh et al. This is an open access article distributed under the terms of the [Creative Commons Attribution License](https://creativecommons.org/licenses/by/4.0/), which permits unrestricted use, distribution, and reproduction in any medium, provided the original author and source are credited.

Data Availability Statement: All relevant data are within the paper and its Supporting Information files.

Funding: This project was supported by grants from the Fondation de France, the Institut National du cancer/Direction Générale de l'Offre de Soins (INCa/DGOS), the French Cancéropôle Nord-Ouest (CNO) and the Fondation ARC pour la recherche sur le cancer. OS was funded by a fellowship from the French Ministry of Education. The funders had no role in study design, data collection and analysis, decision to publish, or preparation of the manuscript.

Abstract

The identification of a causal mutation is essential for molecular diagnosis and clinical management of many genetic disorders. However, even if next-generation exome sequencing has greatly improved the detection of nucleotide changes, the biological interpretation of most exonic variants remains challenging. Moreover, particular attention is typically given to protein-coding changes often neglecting the potential impact of exonic variants on RNA splicing. Here, we used the exon 10 of *MLH1*, a gene implicated in hereditary cancer, as a model system to assess the prevalence of RNA splicing mutations among all single-nucleotide variants identified in a given exon. We performed comprehensive minigene assays and analyzed patient's RNA when available. Our study revealed a staggering number of splicing mutations in *MLH1* exon 10 (77% of the 22 analyzed variants), including mutations directly affecting splice sites and, particularly, mutations altering potential splicing regulatory elements (ESRs). We then used this thoroughly characterized dataset, together with experimental data derived from previous studies on *BRCA1*, *BRCA2*, *CFTR* and *NF1*, to evaluate the predictive power of 3 *in silico* approaches recently described as promising tools for pinpointing ESR-mutations. Our results indicate that $\Delta tESRseq$ and ΔHZ_{EI} -based approaches not only discriminate which variants affect splicing, but also predict the direction and severity of the induced splicing defects. In contrast, the $\Delta \Psi$ -based approach did not show a compelling predictive power. Our data indicates that exonic splicing mutations are more prevalent than currently appreciated and that they can now be predicted by using bioinformatics methods. These findings have implications for all genetically-caused diseases.

Competing Interests: The authors have declared that no competing interests exist.

Author Summary

The biological interpretation of most disease-associated variants has become a real challenge, especially with the implementation of next-generation sequencing. Particular attention is typically given to protein-coding changes often neglecting the potential impact of exonic variants on RNA splicing. Here, we used the exon 10 of *MLH1*, a gene implicated in hereditary cancer, as a model system to assess the prevalence of RNA splicing mutations among all single-nucleotide variants identified in a given exon by using minigene-based assays. Our study revealed an unexpected high proportion of splicing mutations in *MLH1* exon 10 mostly affecting potential exonic splicing regulatory elements (ESRs), which are typically difficult to predict by using *in silico* tools. We then used five experimental data-sets (*MLH1*, *BRCA1*, *BRCA2*, *CFTR* and *NF1*) to evaluate the predictive power of 3 *in silico* approaches recently described for pinpointing ESR-mutations. What's more, besides predicting which exonic variants affect splicing, ΔESRseq and $\Delta\text{HZ}_{\text{EI}}$ values also indicated the direction and severity of the induced splicing defects. In contrast, the $\Delta\Psi$ -based approach did not show a compelling predictive power. Our data indicates that exonic splicing mutations are more prevalent than currently appreciated and that they can now be predicted by using bioinformatics methods. These findings have implications for all genetically-caused diseases.

Introduction

Tremendous progress has been made in recent years in high-throughput technologies enabling fast and affordable massive parallel DNA sequencing. These methods are now being implemented both in molecular diagnostic settings and in basic research laboratories and hold great promise for discovering the genetic bases of rare and complex diseases [1]. However, even if next-generation sequencing has greatly improved the detection of nucleotide changes in the genome of each individual, the biological and clinical interpretation of most variants remains challenging, representing one of the major hurdles in current medical genetics [2,3]. Several reasons account for the difficulty in distinguishing which variants may cause or contribute to disease [4,5]: (i) the number of single-nucleotide variants (SNVs) detected in each genome is very high, (ii) many disorders are genetically heterogeneous and often caused by rare variants, (iii) access to clinical and family data, such as pedigrees, is frequently limited, (iv) *in silico* tools aiming at identifying deleterious changes are still imperfect, and (v) biological samples from variant carriers are rarely available for functional analysis. There is obviously a great need for overcoming these limitations, and considerable efforts are now deployed for developing strategies allowing prioritization of variants for functional testing [4,6].

In general, scrupulous attention is given to exonic SNVs mapping to protein coding regions, especially to those producing missense changes. Indeed, one of the most widely used strategies for narrowing down the number of variants susceptible of causing disease is to use a combination of *in silico* tools that focus on protein features (such as PolyPhen-2, SIFT and Mutation Assessor, among others) [7–9]. Yet, such protein-centric view of the exome landscape merely represents a fraction of the “expression code” underlying each gene sequence. Current knowledge clearly indicates that, besides their protein coding potential, exonic sequences can play an important role in RNA splicing (reviewed in [10,11]). Notably, (i) the first and the last 3 exonic positions are an integral part of 3' and 5' splice site (3'ss and 5'ss) consensus sequences, and (ii) exons may also contain splicing regulatory elements (ESRs), such as exonic splicing enhancers (ESEs) and exonic splicing silencers (ESSs). ESEs and ESSs usually correspond to 6–8

nucleotide stretches that serve as landing pads for splicing activator or splicing repressor proteins, respectively, thereby influencing the recruitment and activity of the splicing machinery. Whereas 3'ss and 5'ss consensus sequences have been extensively characterized leading to the development of *in silico* tools that reliably predict alterations in splice site strength (such as MaxEntScan, SpliceSiteFinder-like and Human Splicing Finder, among others), ESRs are still poorly understood and generally regarded as difficult to predict by using bioinformatics approaches [12–15].

Lately, three new *in silico* approaches were described as promising tools to predict variant-induced ESR alterations. The first approach relies on ESRseq scores established through experimental assessment of the ESR properties of all possible 6-nucleotide motifs [16]. Calculation of total ESRseq score changes (ΔESRseq), taking into account overlapping hexamers and variant-induced changes, was then implemented by our group as a tool to predict the impact on splicing produced by exonic variants [17]. The second approach is based on Z_{EI} scores derived from a RESCUE-type analysis that computed the relative distribution of hexamer motifs in exons and introns [18]. According to this study, the value of total HZ_{EI} score changes ($\Delta\text{HZ}_{\text{EI}}$, also corresponding to overlapping hexamers) can be applied for predicting the impact on splicing of any exonic variant. The third and last approach relies on $\Delta\Psi$ values (Ψ , percent spliced in) that were bioinformatically established upon compilation of RNAseq data obtained from different tissues, and integration of a large set of pre-established sequence features [19]. The $\Delta\Psi$ -based approach was developed to predict splicing aberrations induced by any sequence change, either intronic or exonic, including variants affecting splice sites or splicing regulatory signals.

Today, it is estimated that ~15% of all point mutations causing human inherited disorders disrupt splice-site consensus sequences, particularly at intronic positions [20]. Yet, it is now speculated, based on *in silico* data, that disease-causing aberrant RNA splicing may be more widespread than currently appreciated, with up to 25% of exonic disease-associated variants being expected to disturb ESRs [11,21]. Here, we decided to use the exon 10 of the *MLH1* gene as a paradigm to experimentally evaluate these assumptions. *MLH1* exon 10 was selected as model system for 3 main reasons: (i) *MLH1* is the major gene implicated in Lynch syndrome, one of the most frequent forms of hereditary cancer worldwide, formerly known as hereditary nonpolyposis colorectal cancer (HNPCC), (ii) this gene exhibits a large mutational spectrum, with at least 30% of variants being currently classified as variants of unknown significance and for which large national and international efforts persist in bringing clarification [22,23], and (iii) alterations of potential ESRs were already reported for 3 SNVs in this exon [13,24].

We retrieved all SNVs identified in *MLH1* exon 10 and analyzed their impact on splicing by resorting to both minigene-based assays and analysis of patient's RNA when available. Moreover, we used our experimental data to perform a comparative analysis of the 3 newly developed *in silico* tools aiming at predicting variant-induced ESR alterations. Our results revealed an unexpected high number of splicing mutations in *MLH1* exon 10, most of which affecting potential ESRs, thus corroborating our initial hypotheses. Moreover, we confirmed the predictive power of ΔESRseq - and $\Delta\text{HZ}_{\text{EI}}$ - based approaches, but not that of $\Delta\Psi$, for pinpointing this type of mutations.

Results

Identification of an unexpected high proportion of splicing mutations in the exon 10 of *MLH1*

We have recently shown that a high number of variants (15 out of 36, i.e. 42%) identified in the exon 7 of the *BRCA2* gene have a negative impact on splicing [17], a finding strongly suggesting that either *BRCA2* exon 7 is exceptionally sensitive to exonic splicing mutations, or that this

type of mutations is more frequent than currently estimated. To test these hypotheses, we decided to study the impact on splicing of SNVs identified in another gene, more specifically in *MLH1*, a gene implicated in Lynch syndrome. Our approach was to use the exon 10 of *MLH1* as a model system. We began by interrogating National and International public databases in order to retrieve all single substitutions reported in this exon (Table 1 and Fig 1A). As a result, we found a total of 22 SNVs, most of which identified in cancer patients suspected of Lynch syndrome, including 15 missense, 3 nonsense and 4 synonymous variants. Only 9 of these SNVs are currently classified as clearly pathogenic, and 1 as clearly not pathogenic (Table 1). To assess the impact of all 22 variants on *MLH1* exon 10 splicing, we performed an *ex vivo* splicing assay with pSPL3m-M1e10-derived minigenes (Fig 1B). As shown on Figs 1C and S1, the wild-type pSPL3m-M1e10 minigene predominantly generated transcripts containing exon 10 (79% exon inclusion), and a minority of transcripts without exon 10. These results are in agreement with those previously reported by using the same minigene system [13], and indicate that wild-type pSPL3m-M1e10 mimics, at least in part, the alternative splicing pattern of endogenous *MLH1* transcripts [25–27] (~35% to 67% exon 10 inclusion in normal blood samples, according to a study from Charbonnier and collaborators [25]). Importantly, the minigene assay results revealed that 17 out of the 22 SNVs (77%) altered the splicing pattern of exon 10 relative to wild-type (Figs 1C and S1). More precisely, 13 variants increased exon skipping, 4 variants increased exon inclusion, and only 5 variants showed no effect on splicing. Of

Table 1. *MLH1* exon 10 variants analyzed in this study. *MLH1* exon 10 spans nucleotide positions c.791 to c.884. The first and the last 3 exonic positions (delineated by the dashed line) are an integral part of the 3' ss and 5' ss consensus sequences, respectively. LOVD, Leiden Open Variation Database; dbSNP, the Single Nucleotide Polymorphism database; UMD-*MLH1*, Universal Mutation Database-*MLH1*; Swiss-Prot, the European protein sequence database. Variant classification was retrieved from the LOVD database and refers to the 5-tier system used by the InSIGHT Variant Interpretation Committee (<http://insight-group.org/variants/classifications/>) as follows: 1, not pathogenic; 2, likely not pathogenic; 3, uncertain; (also called VUS for variants of unknown significance); 4, likely pathogenic; 5, pathogenic; n/a, not available.

Position in <i>MLH1</i> exon 10	Nucleotide variant	Predicted amino acid change	Databases	Variant classification
+1	c.791A>G	p.His264Arg	LOVD, dbSNP	3
+3	c.793C>A	p.Arg265Ser	LOVD, dbSNP	4
+3	c.793C>T	p.Arg265Cys	LOVD, dbSNP, UMD- <i>MLH1</i>	5
+4	c.794G>A	p.Arg265His	LOVD, dbSNP, UMD- <i>MLH1</i>	3
+13	c.803A>G	p.Glu268Gly	LOVD, dbSNP	1
+16	c.806C>G	p.Ser269*	LOVD, dbSNP, UMD- <i>MLH1</i>	5
+24	c.814T>G	p.Leu272Val	LOVD, dbSNP	3
+25	c.815T>C	p.Leu272Ser	LOVD, dbSNP	n/a
+50	c.840T>A	p.Tyr280*	LOVD, dbSNP	5
+52	c.842C>T	p.Ala281Val	LOVD, dbSNP, UMD- <i>MLH1</i>	5
+55	c.845C>G	p.Ala282Gly	LOVD, dbSNP, Swiss-Prot	2
+61	c.851T>A	p.Leu284*	LOVD, dbSNP, UMD- <i>MLH1</i>	5
+65	c.855C>T	p. = (p.Pro285Pro)	LOVD, dbSNP	n/a
+66	c.856A>C	p.Lys286Gln	LOVD, dbSNP	3
+71	c.861C>T	p. = (p.Asn287Asn)	LOVD, dbSNP	3
+85	c.875T>C	p.Leu292Pro	LOVD, dbSNP, Swiss-Prot	3
+92	c.882C>G	p. = (p.Leu294Leu)	LOVD	3
+92	c.882C>T	p. = (p.Leu294Leu)	LOVD, dbSNP, UMD- <i>MLH1</i>	5
+93	c.883A>C	p.Ser295Arg	LOVD, dbSNP	5
+93	c.883A>G	p.Ser295Gly	LOVD, dbSNP	5
+94	c.884G>A	p.Ser295Asn	LOVD, dbSNP	5
+94	c.884G>C	p.Ser295Thr	LOVD, dbSNP, Swiss-Prot	4

doi:10.1371/journal.pgen.1005756.t001

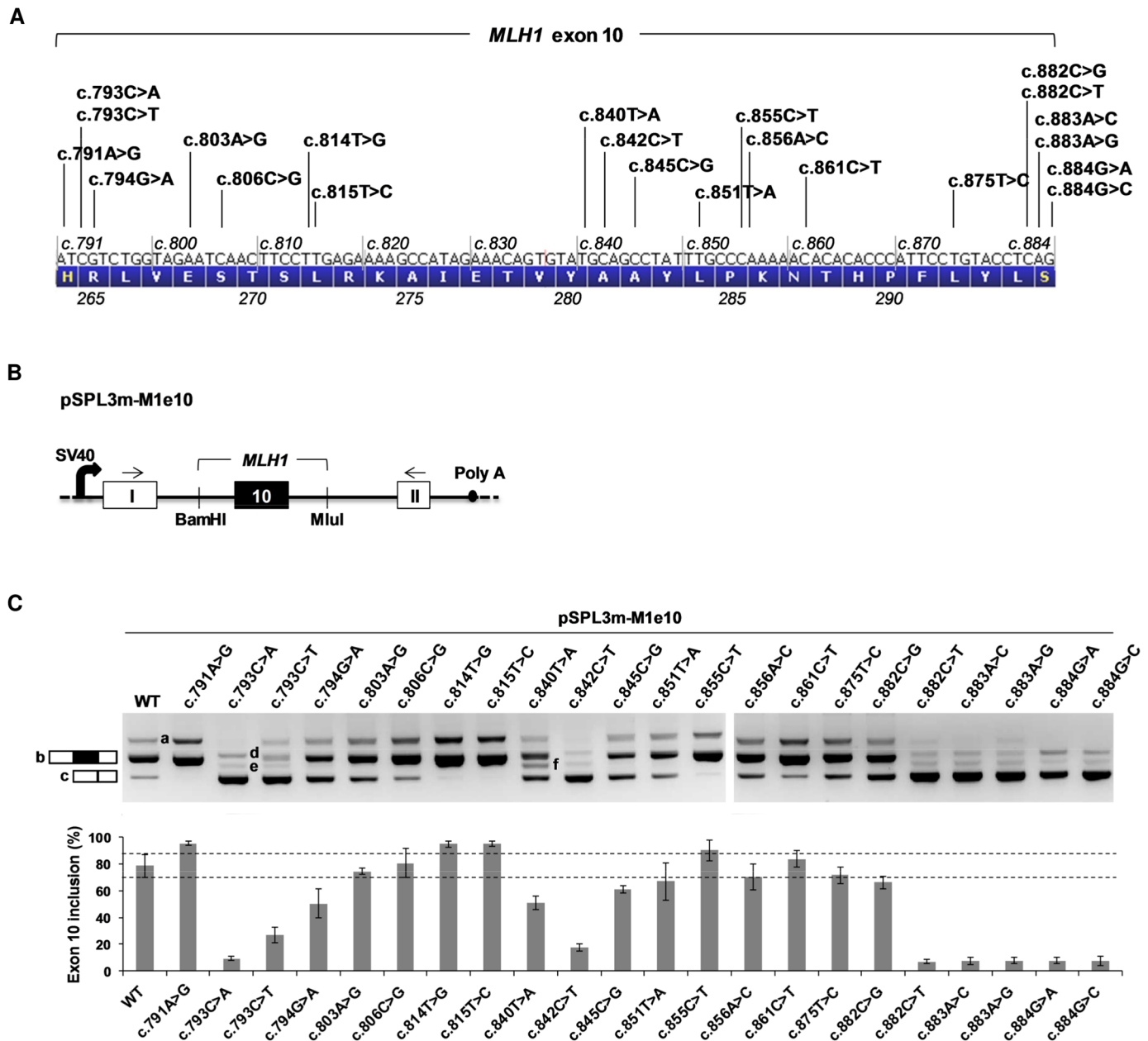


Fig 1. Identification of *MLH1* exon 10 splicing mutations by using a pSPL3m-M1e10 minigene splicing reporter assay. (A) Distribution of all SNVs reported in *MLH1* exon 10 ($n = 22$). The diagram shows the nucleotide composition of *MLH1* exon 10 (c.791-c.884) and the corresponding amino-acid sequence (1-letter code, p.264-p.295), as well as the position and identity of each SNV. (B) Structure of the pSPL3m-M1e10 minigenes used in the splicing reporter assay. Boxes represent exons and lines in between indicate introns. The minigenes were generated by inserting a genomic fragment containing *MLH1* exon 10 and upstream/downstream flanking intronic sequences (168/187 nucleotides, respectively) into the intron of pSPL3m, as described under Materials and Methods. Arrows above the exons represent RT-PCR primers used in the splicing reporter assay. SV40, SV40 promoter; Poly A, polyadenylation site. (C) Analysis of the splicing pattern of pSPL3m-M1e10 minigenes containing the variants indicated in (A). Wild-type (WT) and mutant pSPL3m-M1e10 constructs were transfected into HeLa cells and then the minigenes' transcripts were analyzed by RT-PCR as described under Materials and Methods. The top panel shows the RT-PCR products, obtained for WT and mutant constructs as indicated, separated on a 2.5% agarose gel stained with ethidium bromide. The identities of the two major RT-PCR products, with or without exon 10 (b and c, respectively), are indicated on the left. All the products (a, b, c, d, e and f) are described in detail in S1 Fig, f corresponding to RT-PCR products containing exon 10 deleted of the last 48 nucleotides. The bottom panel shows the quantification of the RT-PCR products. Results are shown as the average of three independent experiments and are expressed as percentage of exon inclusion ($[(\text{exon inclusion products (a+b)} \times 100) / \text{total transcripts}]$). Error bars indicate individual standard deviation (SD) values, whereas the horizontal dashes delineate the limits of the SD bar obtained for WT (79 ± 9 ; i.e. 70% and 88% exon inclusion). Variants producing exon inclusion levels outside this range were considered as splicing mutations.

doi:10.1371/journal.pgen.1005756.g001

note, 8 of the 13 exon-skipping mutations (5 missense, 1 synonymous, and 2 nonsense) are currently classified as pathogenic (Table 1). The 13 variants increasing exon 10 skipping can be separated into three categories according to the severity of the splicing defect observed in the pSPL3m-M1e10 minigene assay: a first category consisting of 6 variants causing near-total exon skipping (7% to 9% exon inclusion: c.793C>A, c.882C>T, c.883A>C, c.883A>G, c.884G>A and c.884G>C; S1 Table and S3B Fig), a second category consisting of five variants inducing moderate skipping (26% to 67% exon inclusion: c.793C>T, c.794G>A, c.845C>G, c.851T>A and c.882C>G, S1 Table) and a third category consisting of 2 variants (c.840T>A and c.842C>T) that led not only to increased exon 10 skipping (51% and 18% exon inclusion, respectively, S1 Table) but also to deletion of the last 48 nucleotides of the exon in a small fraction of the minigene transcripts (S1B Fig, right panel). A bioinformatics analysis using splice site-dedicated algorithms revealed that both variants, c.840T>A and c.842C>T, create a 5' splice site at exonic position +46 (*MLH1* c.836, S1C Fig), which explains the 48-nucleotide deletion at the end of the exon but not the predominant exclusion of the entire exon.

To gain further insight into the severity of the splicing defects of the 13 mutants that induced exon 10 skipping in pSPL3m-M1e10, we tested these variants in the context of another splicing reporter minigene, pCAS2-M1e10 (S2 Fig), previously shown to be less sensitive to splicing mutations than pSPL3m-M1e10 [13]. Our results indicate that, in contrast to pSPL3m-M1e10 and as expected, wild-type pCAS2-M1e10 exclusively generated transcripts containing exon 10. We also observed that 5 out of 6 variants from the first category exhibited a behavior similar to the one observed with the pSPL3m minigenes, i.e. near-total exon 10 skipping; the exception being c.882C>T that induced partial, though strong, exon 10 skipping in the pCAS2 system. Four out of 5 variants from the second category showed splicing defects less severe than the ones observed with pSPL3m-M1e10 and, in one case, c.851T>A, no splicing anomaly was detected. One should note that the level of exon skipping induced by this last variant was borderline noticeable in the pSPL3m-derived minigene (Fig 1C and S1 Table). As for the third category group, we observed that the splicing defects detected in the pSPL3m minigene were faithfully reproduced in pCAS2 for one of the variants (c.842C>T, which predominantly yielded exon-skipped products) but not for the other (c.840T>A). The fact that, in the pCAS2 system, c.840T>A predominantly produced transcripts containing exon 10 deleted of its last 48 nucleotides and almost no exon-skipped products (S2 Fig) suggests that the type and severity of the splicing defect caused by this variant depends on surrounding nucleotide context.

We surmise, given their position at the termini of the exon, that 7 out of the 17 splicing mutations detected in exon 10 directly affect the definition of the reference splice sites, either at the level of the 3' splice site (YAG | G, first exonic position underlined) or of the 5' splice site (CAG | GURAGU, 3 last exonic positions underlined) [10]. Accordingly, the effects produced by these 7 variants (c.791A>G, c.882C>G, c.882C>T, c.883A>C, c.883A>G, c.884G>A and c.884G>C) could have been predicted by algorithms commonly used to predict the strength of splice sites, such as Splice Site Finder, MaxEntScan, and Human Splice Finder (HSF-ss). As shown on S3 Fig, *in silico* data derived from these programs strongly suggest that c.791A>G improves exon inclusion by directly increasing the strength of the 3' splice site, and that the variants at the last three positions of the exon (c.882 to c.884), induce exon skipping by decreasing, to different extents, the strength of the 5' splice site. Moreover, according to this bioinformatics analysis, especially with MaxEntScan (MES), one could have correctly predicted that the splicing defect produced by c.882C>G is less severe than the one induced by c.882C>T. Our data further indicates that a decrease in 5'ss MES score of $\geq 19\%$ predicts very drastic exon 10 skipping.

Because the 10 remaining splicing mutations detected in *MLH1* exon 10 are located outside the positions directly defining the splice sites, we strongly suspect that they interfere with exon recognition by altering ESRs. This type of splicing mutations includes variants that map within the first two thirds of exon 10 and are responsible for inducing either exon skipping (c.793C>A, c.793C>T, c.794G>A, c.840T>A, c.842C>T, c.845C>G and c.851T>A) or exon inclusion (c.814T>G, c.815T>C and c.855C>T).

Detection of potential splicing regulatory elements in the exon 10 of *MLH1*

To better understand how *MLH1* exon 10 splicing is regulated and how certain SNVs disturb this process, we decided to functionally characterize different regions of the exon in the context of pcDNA-Dup. This three-exon minigene contains a middle exon particularly sensitive to alterations of splicing regulatory elements [13,17,28]. For this purpose, four partially overlapping segments covering the entire exon 10 of *MLH1* (R1 to R4, ~30 bp-long each) were individually inserted into the middle exon of this construct and then tested in the context of an *ex vivo* splicing assay (Fig 2A and 2B). As shown in Fig 2C, our results revealed that region R1 (*MLH1* c.791-819) strongly contributed to the recognition of the middle exon. Regions R2 (c.809-c.840), R3 (c.828-c.859) and R4 (c.856-c.884) had a positive effect on exon inclusion as well, although more moderate for R2 and R3 (in comparison to R1), and weak for R4. Next, we tested all *MLH1* exon 10 splicing mutations suspected of altering splicing regulatory elements (n = 10, Fig 2A). Importantly, we found that 8 out of these 10 variations altered the splicing efficiency of the middle exon relative to wild-type (Fig 2D). Variants c.793C>A and c.793C>T (both tested in the context of the R1 segment) induced exon skipping, with c.793C>A having an effect stronger than c.793C>T and thus faithfully recapitulating the defects initially detected in pSPL3m-M1e10 and pCAS2-M1e10 minigene assays. The impact on splicing of variants c.814T>G and c.815T>C was also reproduced in the context of pcDNA-Dup as both variants led to an increase in middle exon inclusion (R2 segment). Finally, variants c.840T>A, c.842C>T, c.845C>G and c.851T>A induced middle exon skipping (R3 segment), with c.842C>T having the more pronounced effect, reminiscent of the effects observed in the pSPL3m-M1e10 and pCAS2-M1e10 assays. Results obtained with c.793C>T and c.842C>T agree with those previously reported by using the pcDNA-Dup system [13]. In contrast, we found that the splicing alterations induced by c.794G>A and c.855C>T in the context of pSPL3m-M1e10 minigene could not be reproduced in the pcDNA-Dup assay. As shown on Fig 2D, c.794G>A did not induce middle exon skipping (R1 segment), and c.855C>T did not lead to an increase in exon inclusion (R3 segment), on the contrary, it slightly increased middle exon skipping. We hypothesize that the effect on splicing of these particular variants depends on surrounding nucleotide context. In conclusion, these experiments point to an apparent asymmetry in the distribution of ESRs in *MLH1* exon 10, with a potential ESE-enrichment at the 5' portion, corresponding to about the first 2/3 of the exon, and/or an ESS-enrichment towards the 3' end. Moreover, the evidence of portability, i.e. that the splicing defects caused by most of the analyzed SNVs can be reproduced in a completely heterologous system, further supports the hypothesis that these variants modify *bona fide* splicing regulatory elements.

Bioinformatics approaches based on Δ tESRseq or on Δ HZEI can predict which exonic variants affect splicing regulatory elements

Three independent *in silico* approaches based on the calculation of either Δ tESRseq [17], Δ HZEI [18], or $\Delta\Psi$ [19] values were recently described as promising tools for predicting variants that potentially modify splicing regulatory elements. Because it remained to be determined

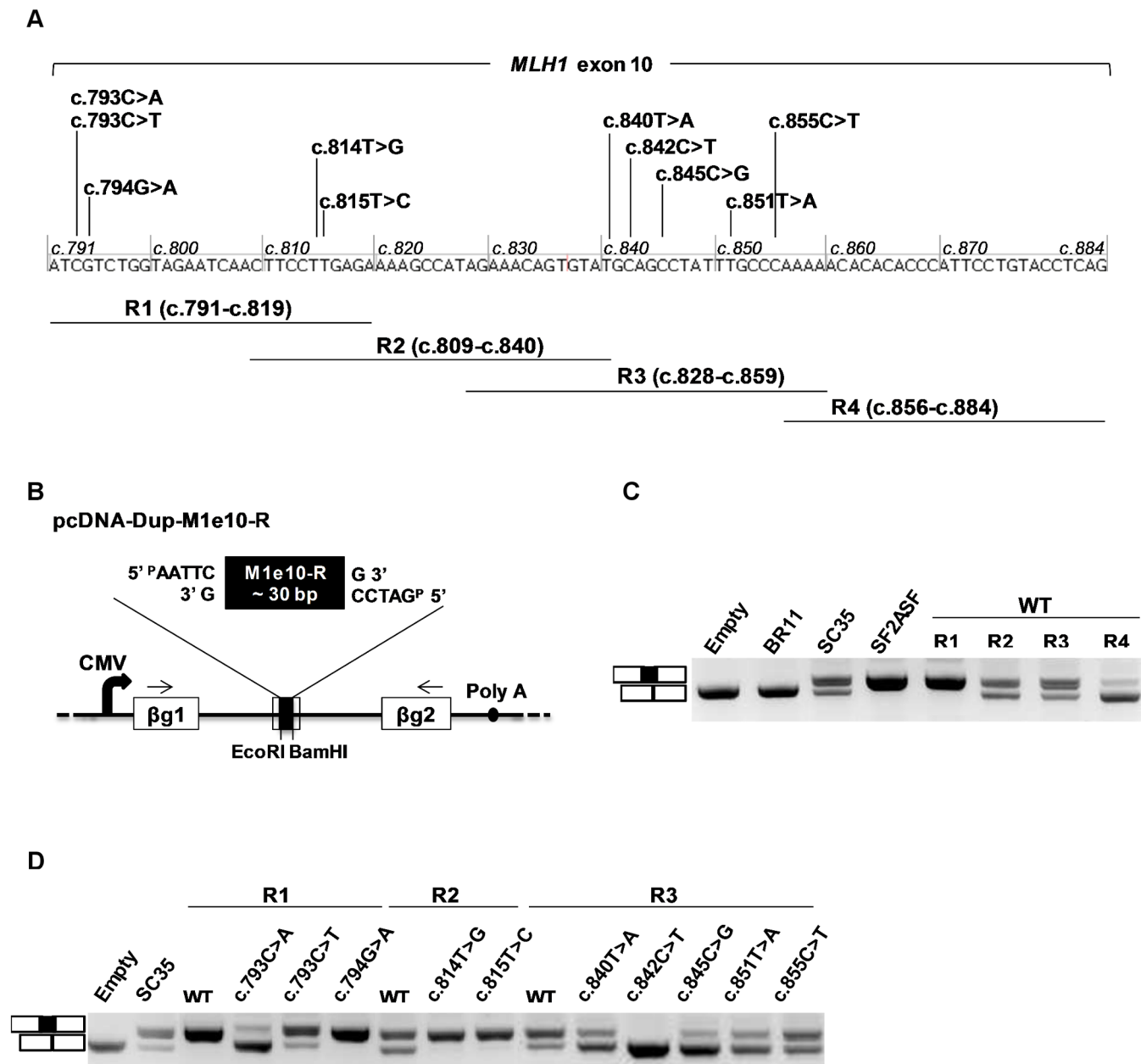


Fig 2. Characterization of *MLH1* exon 10 variants affecting potential ESRs by using an ESR-dependent minigene assay. (A) Strategy for mapping potential splicing regulatory regions in *MLH1* exon 10. The horizontal bars under the sequence of *MLH1* exon 10 represent the ~30 bp-long exonic fragments tested in the ESR-dependent minigene reporter assay (R1 to R4, nucleotide coordinates as indicated). Variants selected for ESR-dependent analysis are indicated above the exon. (B) Structure of the pcDNA-Dup-M1e10-R minigenes used in the ESR-dependent reporter assay. Minigenes were prepared by inserting individual wild-type or mutant *MLH1* exon 10 fragments (M1e10-R as indicated) into the middle exon of pcDNA-Dup, a three-exon vector with a central exon particularly sensitive to ESRs. Boxes indicate exons and lines in between indicate introns. Arrows above the exons represent RT-PCR primers used in the ESR-dependent reporter assay. CMV, CMV promoter; Poly A, polyadenylation site; βg1 and βg2, β-globin exons 1 and 2. (C) Analysis of the splicing pattern of pcDNA-Dup-M1e10-R minigenes containing different wild-type (WT) *MLH1* exon 10 fragments, as indicated. After transfection into HeLa cells the minigenes' transcripts were analyzed by RT-PCR as described under Materials and Methods. The image shows the RT-PCR products separated on a 2.5% agarose gel stained with ethidium bromide and is representative of 3 independent experiments. The identities of the RT-PCR products are indicated on the left. Empty, BR11, SC35 and SF2ASF refer to previously described negative and positive control pcDNA-Dup minigenes [13]. (D) Comparative analysis of the splicing pattern of pcDNA-Dup-M1e10-R minigenes containing either wild-type or mutant *MLH1* exon 10 fragments, as indicated. The assay was performed as described in (C). The image shows the RT-PCR products separated on a 2.5% agarose gel stained with ethidium bromide and is representative of 3 independent experiments. WT, wild-type.

doi:10.1371/journal.pgen.1005756.g002

if these tools could be applied to new cases and how they compare to each other, we next decided to evaluate their performance by using the output of the pSPL3m-M1e10 minigene assay as a new dataset. We started by separating the fifteen *MLH1* exon 10 SNVs located at distance from the splice sites into three groups based on the minigene results (S1 Table). The first group included mutations that increased exon 10 skipping ($n = 7$), the second group included variations with no effect on exon 10 splicing ($n = 5$) and the third group included those that increased exon 10 inclusion ($n = 3$). Then, score differences ($\Delta\text{tESRseq}$, $\Delta\text{HZ}_{\text{EI}}$, and $\Delta\Psi$) were calculated for each variant and plotted in a parallel fashion in order to easily confront the discriminating power of the three bioinformatics approaches (Fig 3). Visual inspection of the plots revealed a striking distribution of $\Delta\text{tESRseq}$ clearly distinguishing the 3 groups of variants. More specifically, most variants with no effect on exon 10 splicing seemed to display $\Delta\text{tESRseq}$ values higher than those increasing exon skipping and lower than those increasing exon inclusion. This feature was not so clearly noticeable for $\Delta\text{HZ}_{\text{EI}}$ or $\Delta\Psi$. A statistical analysis further confirmed that $\Delta\text{tESRseq}$ values were overall concordant with the separation of variants in 3 groups according to minigene data (ANOVA test, p -value of 0.03), whereas $\Delta\text{HZ}_{\text{EI}}$ and $\Delta\Psi$ were not (ANOVA test, p -values of 0.15 and 0.59, respectively) (Fig 3 and S1 Table).

To better assess the performances of the three *in silico* approaches, we set preliminary upper and lower thresholds for predicting variant-induced exon skipping and variant-induced exon inclusion: -0.5 and +0.5 for $\Delta\text{tESRseq}$, -20 and +20 for $\Delta\text{HZ}_{\text{EI}}$, and -0.05 and +0.05 for $\Delta\Psi$ [19], respectively (Fig 3). As a consequence, score differences (Δ) smaller than the pre-established negative thresholds were considered indicative of increased exon skipping, whereas those higher than the positive thresholds were considered indicative of increased exon inclusion. We then determined the relative number of true calls produced by each *in silico* approach giving a particular attention to predictions of exon skipping, the most dreaded variant-induced splicing defect. As shown in Fig 3 and S1 Table, we observed that the $\Delta\text{tESRseq}$ approach produced the highest number of true calls, outperforming $\Delta\text{HZ}_{\text{EI}}$ and $\Delta\Psi$ in discriminating variants that induce exon skipping from those that do not. More specifically, one can reckon 13 (87%) true calls for $\Delta\text{tESRseq}$ against 9 (60%) true calls for both $\Delta\text{HZ}_{\text{EI}}$ and $\Delta\Psi$. Overall, our results revealed a better sensitivity (86% versus 57%) and specificity (88% versus 63%) for $\Delta\text{tESRseq}$ than for $\Delta\text{HZ}_{\text{EI}}$ (S1 Table). In spite of displaying a level of specificity similar to $\Delta\text{tESRseq}$ (88%), $\Delta\Psi$ showed a very high false negative rate (29% sensitivity). Finally, a statistical analysis further confirmed that $\Delta\text{tESRseq}$ values could discriminate variants that increased *MLH1* exon 10 skipping from those that did not, whereas $\Delta\text{HZ}_{\text{EI}}$ and $\Delta\Psi$ could not (t-test, p -values of 0.01, 0.11 and 0.42, respectively).

Results discordant with experimental data, such as the $\Delta\text{tESRseq}$ values obtained for *MLH1* c.845C>G and c.855C>T (outliers in Fig 3) may be due to features not taken into account by the *in silico* approach such as the RNA secondary structure, the chromatin structure, the presence of ESRs longer than six nucleotides, or to a crosstalk with other splicing regulatory elements located nearby.

Next, we wondered if these bioinformatics methods could predict the severity of the splicing defects, i.e. if there was a correlation between the level of exon inclusion detected in the pSPL3m-M1e10 assay and the score differences produced by the $\Delta\text{tESRseq}$, $\Delta\text{HZ}_{\text{EI}}$ and $\Delta\Psi$ approaches. To answer this question, we plotted the minigene data against the score differences generated by the *in silico* approaches, and performed a regression analysis with both variables. As shown on Fig 4 and S1 Table, our results revealed a linear distribution of the *in silico* score differences as a function of exon inclusion levels for $\Delta\text{tESRseq}$ and $\Delta\text{HZ}_{\text{EI}}$ but not for the $\Delta\Psi$ approach (Pearson correlation, p -values of 0.001, 0.004 and 0.93, respectively).

Then, we decided to compare the performance of these three new ESR-dedicated *in silico* tools with that of three previously used methods, more precisely EX-SKIP [29], ESEfinder

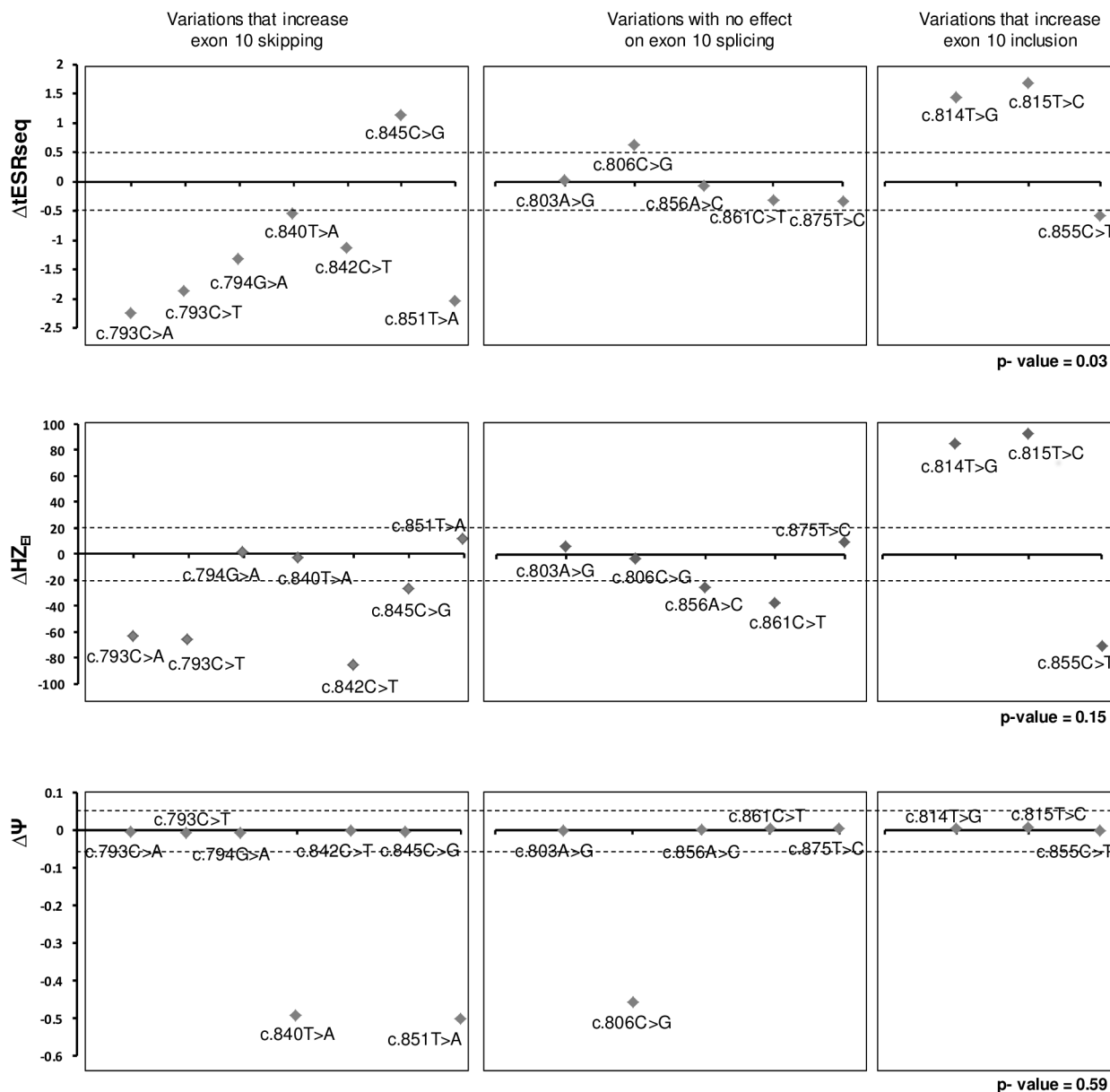


Fig 3. Comparison of pSPL3m-M1e10 minigene data with results obtained from new ESR-dedicated bioinformatics tools. Top, middle and bottom panels refer to results obtained with $\Delta tESRseq$, ΔHZ_{EI} , and $\Delta \Psi$ -based bioinformatics approaches, respectively, as described under Materials and Methods. *MLH1* exon 10 variants located within the sequences that define the reference splice sites were eliminated from this analysis. Retained variants were separated into 3 groups depending on their impact on splicing as determined on the pSPL3m-M1e10 minigene assay and indicated above the graphs. Dashed lines indicate the thresholds used in this study. P-values were calculated by using the one-way ANOVA test, as described under Materials and Methods.

doi:10.1371/journal.pgen.1005756.g003

[30,31] and HSF-SR [32]. As shown in S2 Table, EX-SKIP displayed relatively high specificity (75%) but low sensitivity (43%) in predicting exon-skipping mutations. Statistical analyses further revealed that EX-SKIP could not significantly distinguish *MLH1* exon 10 variants that had an effect on splicing from those that did not (t-test and ANOVA test, p-values of 0.22 and 0.26, respectively). Still, we found that there was a correlation between the level of exon 10 inclusion and EX-SKIP values (Pearson correlation, p-value of 0.02). Data derived from ESEfinder, and especially HSF-SR, were difficult to interpret because of the presence of

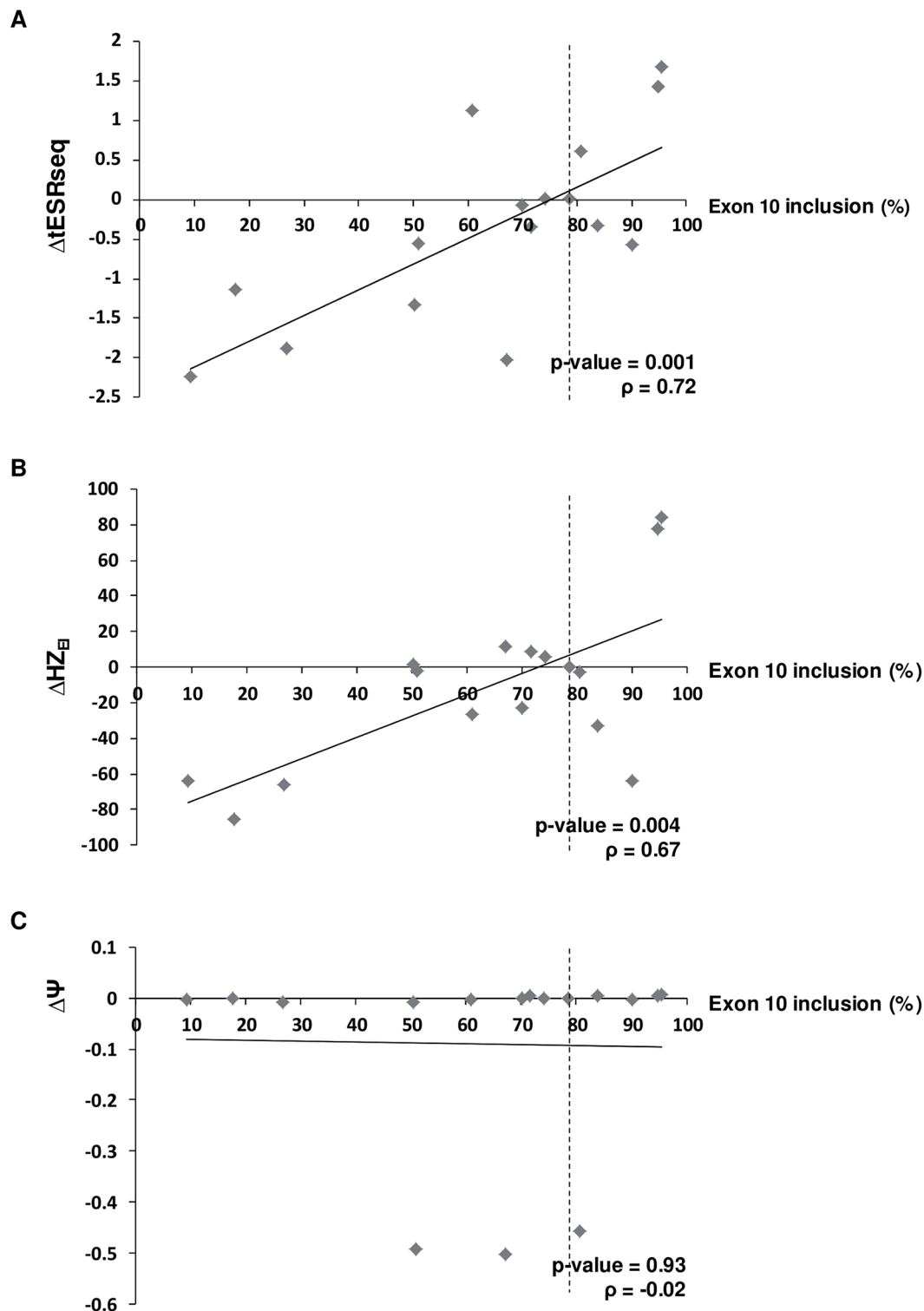


Fig 4. Correlation analysis between exon 10 inclusion levels and results obtained from new ESR-dedicated bioinformatics tools. (A), (B) and (C) refer to results obtained with $\Delta tESRseq$ -, ΔHZ_{EI} - and $\Delta \Psi$ -based bioinformatics approaches, respectively, as described under Materials and Methods. Only *MLH1* exon 10 variants located outside the sequences that define the reference splice sites were retained for this analysis as already mentioned in Fig 3. The precise correspondence between each Δ value ($\Delta tESRseq$, ΔHZ_{EI} or $\Delta \Psi$), the level of exon inclusion observed in the pSPL3m-M1e10 minigene assay, and the identity of the corresponding *MLH1* exon 10 variant, is indicated on S1 Table. Correlation coefficients (r) and p-values were determined by performing a Pearson correlation analysis, as described under Materials and Methods.

doi:10.1371/journal.pgen.1005756.g004

conflicting calls (S2 Table). Moreover, given their lack of comprehensiveness and global quantitation, the performance of these two *in silico* tools could not be statistically analyzed, nor properly compared to that of Δ tESRseq, Δ HZEI, $\Delta\Psi$ or EX-SKIP.

To further evaluate the performance of the recently developed Δ tESRseq, Δ HZEI and $\Delta\Psi$ -based approaches, we extended our study to the dataset that first revealed the predictive potential of Δ tESRseq [17]. This dataset includes a total of 32 *BRCA2* exon 7 variants located outside the reference splice sites, some of which cause exon skipping ($n = 11$, suspected of altering ESRs) and some do not ($n = 21$), as determined experimentally. As shown in S5 Fig and S3 Table, we found again by using this dataset that Δ tESRseq displayed a slightly better sensitivity and specificity than Δ HZEI (in this case, 100% versus 91%, and 86% versus 76%, respectively) whereas $\Delta\Psi$ showed very low sensitivity but high specificity (18% and 94%, respectively). Interestingly, not only Δ tESRseq but also Δ HZEI could distinguish variants that increased exon skipping from those that did not (t-test, p-values of 3.5×10^{-6} and 5.7×10^{-6} , respectively). Again, $\Delta\Psi$ could not discriminate these 2 groups of variants (t-test, p-value of 0.56). Moreover, we observed a statistically significant correlation between the level of *BRCA2* exon 7 inclusion and the score differences produced by the Δ tESRseq and Δ HZEI approaches (Pearson correlation, p-values 1.1×10^{-6} and 0.9×10^{-3} , respectively), whereas $\Delta\Psi$ showed no correlation (Pearson correlation, p-value = 0.15) (S6 Fig and S3 Table). Finally, we completed our study by analyzing three additional datasets experimentally characterized by other laboratories, namely: (i) a set of 42 *BRCA1* exon 6 variants [29], (ii) a set of 41 *CFTR* exon 12 variants [33,34] and (iii) a set of 24 *NF1* exon 37 variants [35]. As shown in S4, S5 and S6 Tables, here again, we found that Δ tESRseq and Δ HZEI had better sensitivity than $\Delta\Psi$ for predicting which variants induce exon skipping (67–100% and 68–100% versus 0–33% sensitivity, respectively, depending on the dataset). Statistical analyses further highlighted the good performance of Δ tESRseq and especially Δ HZEI, but not that of $\Delta\Psi$ for discriminating variants that lead to exon skipping and for predicting the severity of the splicing defect within these 3 additional datasets (S7 Table).

We surmise that out of the three new *in silico* approaches expected to predict ESR-mutations [17–19], Δ tESRseq and Δ HZEI show the best performance at least for the five datasets analyzed in our study. Indeed, these two approaches displayed a better balance between sensitivity and specificity than $\Delta\Psi$, or the prior *in silico* method EX-SKIP, for predicting exon skipping-mutations (S8 Table). Importantly, we found that Δ tESRseq and Δ HZEI can be used to predict not only the direction but also the severity of the induced splicing defects, more negative score differences being indicative of higher exon skipping levels (S7 Table).

***MLH1* c.793C>T and c.842C>T are associated with drastic splicing defects in patients' cells**

To evaluate the physiological pertinence of the *MLH1* exon 10 minigene assays and the above described *in silico* predictions, we set to compare our results with data derived from the analysis of RNA obtained from carriers of *MLH1* exon 10 variants, especially of those located outside splice sites. Patients' RNA being rarely available, we had the opportunity to obtain patient RNA samples for only two SNVs of interest: (i) *MLH1* c.793C>T (Patient P_{793CT.1}) and (ii) *MLH1* c.842C>T (Patient P_{842CT.1}).

First, peripheral blood RNA of patient P_{793CT.1} (heterozygous for *MLH1* c.793C>T) was analyzed by RT-PCR, by using primers targeting exons 8 and 12, and compared to those of three control individuals. Our results revealed a complex splicing pattern involving *MLH1* exons 9, 10 and 11 in all individuals (Figs 5A and S4). These data are concordant with previous studies describing exon 10 as an alternative exon that is naturally partially skipped, either alone or in combination with exon 9 and/or exon 11 [25–27]. We also observed that, as compared to

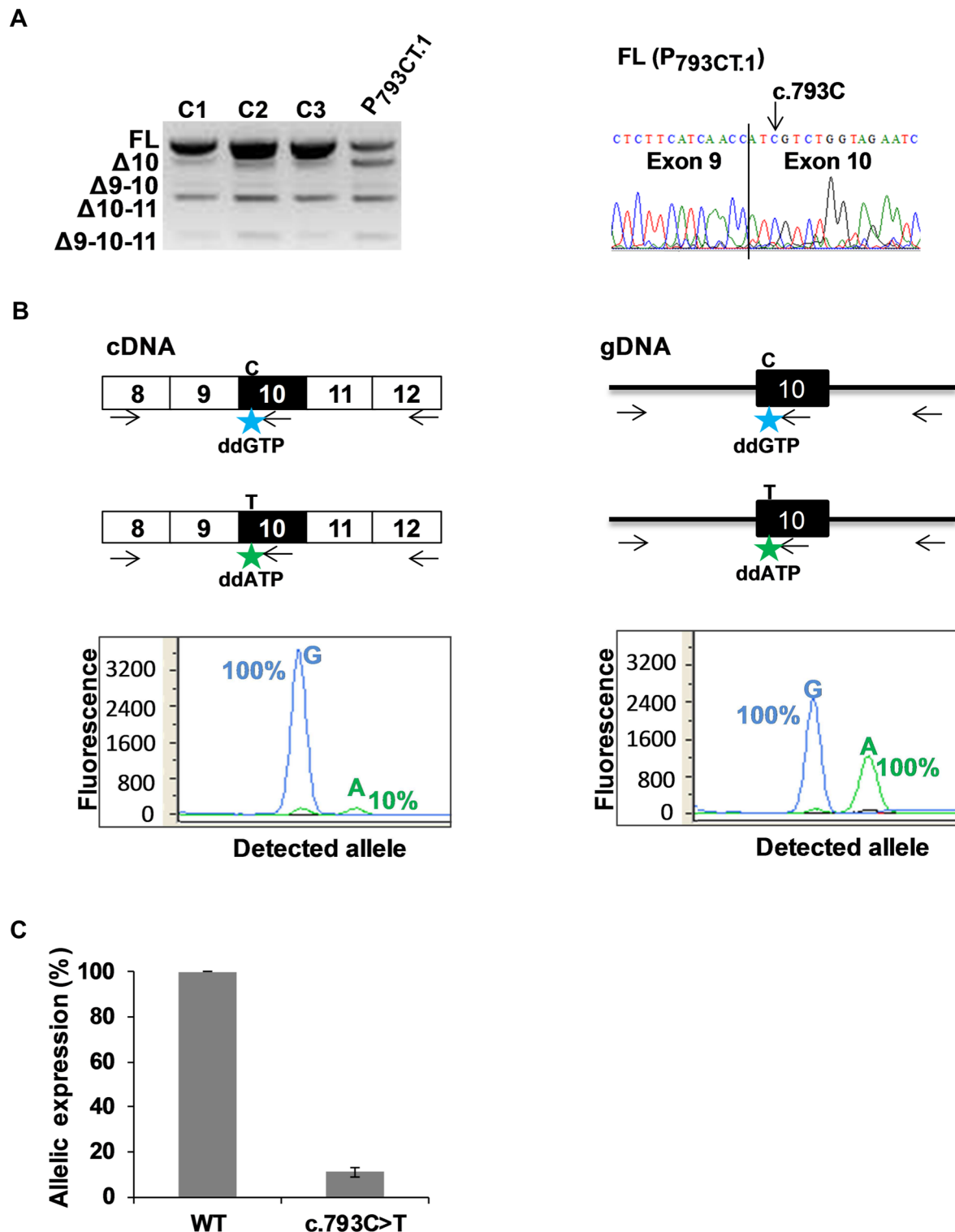


Fig 5. Detection of aberrant splicing in the blood cells of a patient carrying *MLH1* c.793C>T variant. (A) Comparative RT-PCR analysis of fresh blood RNA samples obtained from 3 healthy control individuals (C1, C2 and C3) and from a patient carrying the heterozygous variant *MLH1* c.793C>T (P_{793CT.1}). RT-PCR reactions were performed with primers mapping to *MLH1* exon 8 (forward primer) and exon 12 (reverse primer), as described under Materials and Methods. The panel on the left shows the RT-PCR products separated on a 2% agarose gel, and is representative of 3 independent experiments. RT-PCR product identifiers are indicated on the left of the gel. The sequence on the right refers to the FL product obtained from patient P_{793CT.1}, with a vertical line indicating the junction between exons 9 and 10. FL, full-length; Δ, exon skipping. (B) Allele-specific expression of *MLH1* in the blood cells of patient P_{793CT.1}

carrying the heterozygous variant *MLH1* c.793C>T. PCR, RT-PCR and primer extension reactions were performed as described under Materials and Methods, and are schematically represented above the graphs. The discriminating nucleotides C and T are indicated. Boxes represent exons, lines indicate intronic sequences, and arrows symbolize reaction primers. The discriminating fluorophore-labeled ddG and ddA terminators, incorporated into the noncoding strand at the c.793 position, are represented by stars. Results from complementary DNA (cDNA) analysis and genomic DNA (gDNA) are shown on the left-hand and on the right-hand graphs, respectively. Results (peak areas) obtained with cDNA were normalized to those obtained with gDNA and are expressed, in the left-hand graph, as relative level (in percentage) of FL transcripts produced by each *MLH1* allele. (C) Relative contribution of each allele to the expression of full-length *MLH1* transcripts in the blood cells of patient P_{793CT.1} carrying the heterozygous variant *MLH1* c.793C>T. The graph displays the expression level of the mutant allele (*MLH1* c.793C>T) relative to wild-type (WT). Results are shown as the average of 3 independent experiments performed as described in (B). Error bars indicate standard deviation values.

doi:10.1371/journal.pgen.1005756.g005

controls, the sample derived from patient P_{793CT.1} showed a lower amount of full-length transcripts (FL), and a higher amount of transcripts lacking exon 10 ($\Delta 10$), indicative of aberrant splicing. Sequencing of the FL products revealed the presence of WT (c.793C) exon 10 only (Fig 5A, right panel), which suggests that in this sample the exon 10-skipped products mostly derive from the mutant allele (c.793T), and that the variant-associated splicing defect is very severe. Importantly, the observation that c.793C>T is associated with a drastic splicing defect in endogenous *MLH1* transcripts agrees with the data obtained in the minigene assays (Figs 1, 2 and S2), especially in the context of pSPL3m-M1e10 c.793C>T, which showed a very high level of exon skipping. To better evaluate the consequences of c.793C>T on *MLH1* expression, and because Sanger sequencing is known to have low detection sensitivity, we then decided to measure the relative contribution of the WT and mutant alleles to the production of the full-length (FL) transcripts by using an allele-specific primer extension method. Our findings, shown on Fig 5B and 5C, indicate that the FL transcripts expressed from the mutant allele were in fact present in the blood cells of patient P_{793CT.1} but at very low level as compared to the WT allele (~10%). Given the results of our minigene assays, and RT-PCR analysis of patient's RNA, we conclude that this allelic imbalance is mostly due to c.793C>T-induced exon 10 skipping. Moreover, if one assumes that, in the blood cells of Patient P_{793CT.1}, both alleles are transcribed in equal amounts, then one can deduce that the pSPL3m-M1e10 assay closely reflects the effects detected *in vivo* in patient's peripheral blood, at least for this variant.

We then analyzed LCL RNA from patient P_{842CT.1} (heterozygous for *MLH1* c.842C>T) by comparing to those from 5 controls, including: 3 healthy individuals, and 2 Lynch syndrome patients (P_{791-5TG.1} and P_{882CT.1}) carrying *MLH1* c.791-5T>G and c.882C>T mutations directly altering the 3'ss or 5'ss of exon 10, respectively [36]. Results shown on S7 Fig indicate that patient P_{842CT.1} has a splicing pattern similar to that of patients P_{791-5TG.1} and P_{882CT.1}, i.e. an apparent decrease in the amount of FL *MLH1* transcripts, a mild increase in exon 9–10 skipping ($\Delta 9-10$) and a drastic increase in exon 10 skipping ($\Delta 10$), as compared to healthy controls. $\Delta 10$ transcripts were detected in LCLs treated with puromycin, strongly suggesting that the aberrant $\Delta 10$ out-of-frame transcripts (S4B Fig) are degraded by the NMD pathway in these cell lines. As expected, the level of $\Delta 9-10$ in-frame transcripts did not increase in the presence of the NMD-inhibitor puromycin. Sequencing of the FL RT-PCR products of patients P_{842CT.1} and P_{882CT.1} revealed the absence of c.842T and c.882T mutant FL transcripts (S7C Fig), indicating that c.842C>T and c.882C>T cause very severe splicing defects. These *in vivo* results clearly agree with the pSPL3m and pCAS2 minigene assays, which revealed predominant exon 10 skipping for both c.842C>T and c.882C>T (Figs 1, 2 and S2).

Importantly, these results highlight the physiological pertinence of the *in silico* predictions produced by the Δ tESRseq and Δ HZEI approaches. Indeed, these methods accurately predicted the variant-induced splicing aberrations observed *in vivo* in patients carrying exonic SNVs, as shown here for *MLH1* variants c.793C>T and c.842C>T, and (ii) *BRCA2* c.520C>T or c.617C>G [17,37]. As of note, the Δ tESRseq approach also accurately predicted

the physiological effect of *MLH1* c.794G>A [13]. We conclude that Δ tESRseq and Δ HZ_{EB}, but not Δ Ψ, are promising tools for prioritizing exonic variants for splicing assays.

Discussion

The present study was initiated to follow up on our observation that a large number of variants in the exon 7 of *BRCA2* induce exon skipping [17]. Our hypothesis was that exonic splicing mutations were also underestimated in other exons and genes. We thus decided to analyze the impact on splicing of all SNVs identified in the exon 10 of *MLH1* (n = 22), a gene implicated in Lynch syndrome. Before this study, only 5 SNVs in *MLH1* exon 10 had been reported as causing aberrant splicing; more specifically, they were all shown to increase exon 10 skipping [13,24,36]. Our work not only confirmed those initial findings but, importantly, uncovered 12 new splicing mutations (8 exon skipping-, and 4 exon inclusion-mutations), bringing the number of *MLH1* exon 10 splicing mutations to a total of 17. Hence, our results revealed a striking high proportion of splicing mutations in *MLH1* exon 10 (77%), largely exceeding the fraction of splicing mutations detected in *BRCA2* exon 7 (42%) [17]. Moreover, we found that the majority of *MLH1* exon 10 splicing mutations (~60%) map outside the reference splice-site consensus sequences, indicating an important contribution of variant-induced ESR alterations in this exon.

Importantly, among the 12 new splicing mutations in *MLH1* exon 10, we identified 4 SNVs causing increased exon inclusion. To our knowledge, this is the first report of SNVs having a positive impact on *MLH1* splicing. Besides full-length transcripts, *MLH1* is known to normally produce a fraction of transcripts lacking exon 10, such as Δ 10, Δ 9/10, Δ 10/11 and Δ 9/10/11 [25,26], with Δ 9/10 being one of the most frequently reported alternative *MLH1* isoforms [27]. It is possible that the 4 variants that increased exon 10 inclusion in our minigene assays also disturb *MLH1* physiological alternative splicing leading to a higher production of FL transcripts and lower amount of Δ 10, Δ 9/10 and Δ 9/10/11. Because the role of alternative *MLH1* isoforms is still unknown [27], it is difficult to predict the biological and clinical consequences of these splicing alterations. Of note, a few cases of variant-induced exon inclusion have already been described in other genes. Particularly, previous studies have shown that mutations that increase exon inclusion can have a significant clinical impact. For instance, they can behave as protective factors, as is the case of *SMN2* c.859G>C (p.Gly287Arg), a variant that attenuates the severity of spinal muscular atrophy (SMA) by increasing inclusion of *SMN2* exon 7 [28,38]. Moreover, mutations inducing exon inclusion can also be harmful, as is the case for the majority of mutations identified in the exon 10 of the *Microtubule Associated Protein Tau* gene (*MAPT*) (reviewed in [39]). It has been shown that dysregulation of *MAPT* exon 10 splicing disrupts normal tau isoform ratio and leads to neurodegeneration and dementia: increased *MAPT* exon 10 skipping causes Pick disease, whereas increased inclusion typically causes FTDP-17 (frontotemporal dementia with parkinsonism linked to chromosome 17).

Given the challenging need in medical genetics for stratifying exonic variants for functional analyses, we decided to use the experimental data generated in this study to evaluate the predictive power of *in silico* tools at discerning splicing mutations. We found that the impact on splicing of the seven *MLH1* exon 10 variants mapping within the splice-site consensus sequences (potential splice site-mutations) were correctly predicted by splice site-dedicated *in silico* tools (SSF, MES and HSF-ss). These findings confirm and extend previous studies that highlighted the good reliability of these algorithms for predicting exon skipping-mutations [12–15], further pinpointing their interest as filtering tools in variant stratification strategies. As for the variants located outside the reference splice sites, our minigene data revealed 10 ESR-mutations and 5 variants with no impact on splicing. We took advantage of these results and selected four

additional experimental datasets previously described in other genes [17,29,33–35] to evaluate the discriminating power of 3 bioinformatics approaches recently described as suitable for predicting variant-induced ESR alterations [16–19]. Our findings revealed that the Δ ESRseq and Δ HZ_{EI} ESR-dedicated tools show the best performance in identifying ESR-mutations, outperforming the previous bioinformatics method EX-SKIP, whereas $\Delta\Psi$ did not show compelling predictive power. Our results further indicate that both Δ ESRseq- and Δ HZ_{EI}-based approaches can predict the severity of the variant-induced splicing defects, underlining the quantitative character of these methods. It is possible that the Δ ESRseq- and Δ HZ_{EI}-based approaches produced somewhat similar results because they both rely on the appreciation of hexamer sequences as ESRs. Interestingly, a correlation between ESRseq and Z_{EI} scores has already been reported [18] suggesting that most ESRs are indeed defined by 6-nucleotide stretches and that ESE sequences are more frequently represented in exons than in introns. Contrary to our initial expectations, $\Delta\Psi$ displayed the weakest predictive power out of the 3 new *in silico* tools dedicated to identifying ESR alterations. This was unexpected as this method had been validated by using a large set of previously published splicing data, such as data on a plethora of *MLH1* nucleotide variants [19]. Close inspection of the validation set used on that study revealed a large excess of intronic variants relative to exonic changes, and also a considerable under-representation of known ESR-mutations relative to the total number of variants included in the dataset. Most of the positive predictions reported for $\Delta\Psi$ [19] thus correspond to intronic mutations directly affecting splice sites. This may explain why we detected an excess of true negative calls relative to true positive calls when using $\Delta\Psi$ -values for predicting ESR-mutations in the five datasets analyzed in this study, and suggests that the $\Delta\Psi$ -based method may be overall suitable for predicting mutations directly modifying splice sites but not entirely reliable for predicting those affecting ESRs. In sum, our findings suggest that both Δ ESRseq- and Δ HZ_{EI}-based approaches can be used to stratify exonic variants for functional testing, and that this strategy may help identifying disease-causing variants. We cannot exclude that $\Delta\Psi$ -values may be useful in particular conditions and, conversely, that the Δ ESRseq- and Δ HZ_{EI}-based approaches may not be suitable for the analysis of certain exons or genes.

In the case of *MLH1*, it is clear that severe exon 10 skipping causes Lynch syndrome (reviewed in [27]). Skipping of *MLH1* exon 10 leads to a shifted reading frame, resulting in a premature stop codon in exon 11 (*MLH1* p.His264Leufs*2) and probable degradation of the aberrant transcripts by NMD. Variants inducing total exon 10 skipping cause a drastic loss in FL *MLH1* protein and are therefore considered deleterious. In contrast, the clinical significance of variants inducing partial exon 10 skipping is still unknown. First, it is unclear if the amount of FL transcripts produced in the presence of such variants is enough to fulfill *MLH1* function. Second, it is possible that remaining FL *MLH1* transcripts carrying missense variants lead to production of nonfunctional proteins. Additional analyses are thus necessary to determine the biological and clinical significance of partial exon skipping-variants, including protein assays, assessment of patient clinical history and family data. Given that exon 10 codes for part of an important domain of the *MLH1* protein (interaction with MUTS α) [40], we suspect that SNVs increasing exon 10 inclusion can either have a protective impact if co-occurring with variants showing the opposite effect, or a deleterious effect if introducing a missense change that severely impairs protein function. Thus, in the absence of further information, *MLH1* missense SNVs inducing exon 10 inclusion, as well as those not affecting splicing, should be considered as variants of unknown significance (VUS). In contrast, the clinical classification of synonymous substitutions not affecting RNA splicing can eventually evolve from VUS to likely not pathogenic depending on expert panel assessment [22,23].

In conclusion, our results revealed an unexpected high number of splicing mutations in the exon 10 of *MLH1*, most of which affecting potential ESRs, and confirmed the predictive power

of Δ tESRseq- and Δ HZ_{EL}-based approaches for pinpointing this type of mutations, at least in *MLH1* exon 10, *BRCA2* exon 7, *BRCA1* exon 6, *CFTR* exon 12 and *NF1* exon 37. In principle, the bioinformatics methods described in our study are amenable to automation and, as such, have the potential to be used as filtering tools for identifying disease-causing candidates among the large number of variants detected by high-throughput DNA sequencing.

Materials and Methods

Ethics statement

Written informed consent was obtained from all individuals.

Retrieval of *MLH1* exon 10 variants

We collected all SNVs reported in the exon 10 of *MLH1*, until January 2013, by interrogating the following public databases: UMD-*MLH1* (Universal Mutation Database-*MLH1*, <http://www.umd.be/MLH1/>) [22], LOVD (Leiden Open Variation Database, http://chromium.liacs.nl/LOVD2/colon_cancer/variants.php?select_db=MLH1), dbSNP (the Single Nucleotide Polymorphism database <http://www.ncbi.nlm.nih.gov/SNP/>), and UniProtKB/Swiss-Prot (the European protein sequence database, http://swissvar.expasy.org/cgi-bin/swissvar/result?global_textfield=MLH1) (Table 1 and Fig 1A).

Nomenclature

Nucleotide numbering is based on the cDNA sequence of *MLH1* (NCBI accession number NM_000249.3), c.1 denoting the first nucleotide of the translation initiation codon, as recommended by the Human Genome Variation Society.

Splicing minigene reporter assays

In order to evaluate the impact on splicing of each *MLH1* exon 10 variant, we performed functional assays based on the comparative analysis of the splicing pattern of wild-type and mutant *MLH1* reporter minigenes. These minigenes were prepared by using two different vectors: pSPL3m and pCAS2. The pSPL3m plasmid, a modified version of the exon-trapping vector pSPL3 (Invitrogen) which in turn derives from pSPL1 [41], carries two chimeric exons (here named I and II, both containing rabbit β -globin and HIV *Tat* sequences) separated by an intron containing BamHI and MluI cloning sites (Fig 1B) [13]. Expression of the pSPL3m minigene is driven by the SV40 promoter. The pCAS2 vector carries two exons (here named A and B) with a sequence derived from the human *SERPING1/C1NH* gene, separated by an intron with BamHI and MluI cloning sites (S2A Fig). Expression of the pCAS2 minigene is under the control of a CMV promoter. The pCAS2 is a modified version of the previously described pCAS1 plasmid [13,42]. Two modifications were introduced into the exon A of pCAS2 relative to pCAS1: (i) the first 114 bp of exon A were deleted, and (ii) the *SERPING1/C1NH* translation initiation codon was disrupted by replacing the sequence GATG (initiation codon underlined) by TCAC.

The wild-type genomic fragment *MLH1* c.791-168_c.884+187 (*MLH1* exon 10 and flanking intronic sequences) was inserted into the BamHI and MluI cloning sites of the reporter plasmids pSPL3m and pCAS2, yielding the three-exon hybrid minigenes pSPL3m-M1e10 and pCAS2-M1e10, respectively (Figs 1B and S2A). Minigenes carrying *MLH1* exon 10 variants were prepared by site-directed mutagenesis by using the two-stage overlap extension PCR method [43] and the wild-type pSPL3m-M1e10 construct as template. Then, the mutant amplicons were digested with BamHI and MluI, and introduced into BamHI and MluI cloning sites of the pSPL3m-M1e10 minigene to replace the wild-type fragment. The inserts of all constructs

were sequenced to ensure that no other mutations had been introduced during the cloning process. In some cases, as indicated (S2 Fig), mutant inserts were digested from the pSPL3m-M1e10 minigene with BamHI and MluI and then subcloned into pCAS2.

Next, wild-type and mutant minigenes (1 µg/well) were transfected in parallel into HeLa cells grown at ~60% confluence in 6-well plates using the FuGENE 6 transfection reagent (Roche Applied Science). HeLa cells were cultivated in Dulbecco's modified Eagle medium (Life Technologies) supplemented with 10% fetal calf serum in a 5% CO₂ atmosphere at 37°C. Total RNA was extracted 24 hours after transfection using the NucleoSpin RNA II kit (Macherey Nagel) according to the manufacturer's instructions. Then, the minigene transcripts were analyzed by semi-quantitative RT-PCR (30 cycles of amplification) in a 25 µl reaction volume by using the OneStep RT-PCR kit (Qiagen), 100 ng total RNA, and pSPL3m- or pCAS2-appropriate forward and reverse primers (SD6 and SA2 or pCAS-KO1-F and pCAS-2-R, respectively, as described in [13] and [37]). RT-PCR products were separated by electrophoresis on 2.5% agarose gels containing ethidium bromide and visualized by exposure to ultraviolet light under non-saturating conditions using the Gel Doc XR image acquisition system (Bio-RAD). Semi-quantitative analysis, gel extraction and sequencing of the RT-PCR products were carried out as previously described [42].

ESR-dependent minigene reporter assay

MLH1 exon 10 fragments (~30 bp-long) were analyzed for their splicing enhancer properties by performing a functional assay based on the splicing pattern of the pcDNA-Dup minigene [13]. This vector contains a β-globin-derived three-exon minigene with a middle exon particularly sensitive to the presence of exonic splicing regulatory signals. Expression of the minigene is under the control of the CMV promoter (Fig 2B). The exonic fragments of interest, wild-type or mutant, were obtained by annealing complementary 5'-phosphorylated oligonucleotides carrying 5'-EcoRI and 3'-BamHI compatible ends. Then, the exonic segments were inserted into the EcoRI and BamHI cloning sites of the middle exon of pcDNA-Dup to produce hybrid pcDNA-Dup-M1e10-R minigenes. All constructs were sequenced to ensure that no other mutations were introduced into the middle exon during the cloning process. Transfection, RNA extraction and RT-PCR analysis were performed as described for the splicing minigene reporter assay except that RT-PCR reactions were performed with 150 ng total RNA as template, T7-Pro (5'-TAATACGACTCACTATAGG-3') and Dup-S4-Seq-3R (5'-CGTGCAGCTTGTCACAGTGC-3') as forward and reverse primers respectively, and 28 cycles of amplification. RT-PCR products were analyzed by electrophoresis as described above for the splicing minigene reporter assay.

Bioinformatics predictions of splice site-mutations

Three *in silico* tools were used to predict variant-induced alterations in 3' and 5' splice site strength, namely: SpliceSiteFinder-like (SSF, <http://www.interactive-biosoftware.com>), MaxEntScan (MES, http://genes.mit.edu/burgelab/maxent/Xmaxentscan_scoreseq.html; Maximum Entropy Model) and the splice site module of Human Splicing Finder (here named HSF-ss for splice site-dedicated HSF, <http://www.umd.be/HSF/>). These algorithms were interrogated simultaneously by using the integrated software tool Alamut (Interactive Biosoftware, France, <http://www.interactive-biosoftware.com>), as previously described [17].

Bioinformatics predictions of ESR-mutations

Three newly developed *in silico* approaches were used to predict variant-induced alterations in exonic splicing regulatory elements (ESRs): (i) calculation of total ESRseq score changes

(Δ tESRseq) by using the method previously described by our group [17] with a small modification (here, only exonic positions were taken into account), (ii) calculation of Δ HZ_{EI} values by using the HEXplorer method [18], and (iii) assignment of $\Delta\Psi$ values based on the Splicing Regulatory Model (<http://tools.genes.toronto.edu>) recently described by Xiong and co-workers [19]. Moreover, as indicated, we also resorted to three previously established ESR-dedicated *in silico* tools: (i) EX-SKIP (<http://ex-skip.img.cas.cz/>) [29] in which we took into account the full nucleotide sequence of the exon of interest, (ii) ESEfinder (http://rulai.cshl.edu/cgi-bin/tools/ESE3/ese_finder.cgi?process=home) [30,31], and (iii) the ESR module of Human Splicing Finder (here named HSF-SR for ESR-dedicated HSF, <http://www.umd.be/HSF3/>) [32].

Statistical analysis

Results are presented as the mean \pm SD of three independent experiments. Data derived from comparisons of experimental and *in silico* analyses were compared by using either the one-way ANOVA test or the Student's t-test, and the Pearson's correlation coefficient, as indicated. More specifically, the ANOVA test was used for assessing the performance of the bioinformatics tools in discriminating 3 groups of variants (i.e. variants that increase exon skipping versus those with no effect on splicing versus those that increase exon inclusion), whereas Student's t-test was used when only 2 groups of variants were taken into account (i.e. variants that increase exon skipping versus those that do not). Correlation between exon inclusion levels and *in silico* predictions was measured by calculating Pearson correlation coefficients (r). p-values and r are indicated in the figures. Results were considered significant when p-value < 0.05. Statistical tests were performed by using BiostaTGV (<http://marne.u707.jussieu.fr/biostatgv/>).

The power to distinguish mutations that induce exon skipping from those that do not was further assessed, for each ESR-dedicated *in silico* method, by calculating sensitivity and specificity values (true positives \times 100/(true positives + false negatives) and (true negatives \times 100/(true negatives + false positives), respectively). Sensitivity and specificity were determined by taking into account the following thresholds: -0.5 for Δ tESRseq (arbitrary threshold), -20 for Δ HZ_{EI} (arbitrary threshold), and -0.05 for $\Delta\Psi$ (threshold previously established by the authors, [19]).

Analysis of the splicing pattern of *MLH1* in peripheral blood samples and lymphoblastoid cell lines of patients and controls

Peripheral blood samples were directly collected into PAXgene Blood RNA Tubes (Qiagen) from which total RNA was extracted by using the PAXgene Blood RNA kit, according to the manufacturer's instructions. EBV-immortalized lymphoblastoid cell lines (LCLs) were cultivated in RPMI medium (Life Technologies) supplemented with 2 mM of L-glutamine and 10% fetal calf serum, at 37°C in a 5% CO₂ atmosphere. Before RNA extraction, LCLs were transferred into 6-well plates, at 2.5×10^6 cells/well, and incubated for 5.5 hours with/without 200 μ g/ml puromycin. Then, total RNA was extracted by using the NucleoSpin RNA II kit (Macherey Nagel). Written informed consent was obtained from all individuals.

The splicing pattern of *MLH1* transcripts expressed in peripheral blood and in LCLs was analyzed by semi-quantitative RT-PCR using the OneStep RT-PCR kit (Qiagen) in 25 μ l-final volume reactions containing 100 ng of total RNA, a forward primer located in *MLH1* exon 8 (MLH1-RT-8Fbis, 5'-AAGGAGAGACAGTAGCTGATGTT-3') and a reverse primer located in exon 12 (MLH1-12R, 5'-TGCTCAGAGGCTGCAGAAA-3'). To ensure that the assay was in the linear range, RT-PCR reactions were performed with 34 cycles of amplification (S4 Fig). Then, RT-PCR products were separated by electrophoresis on a 2% agarose gel, gel-purified and sequenced.

Allele specific expression analysis

Allele specific expression (ASE) was measured by performing a SNaPshot assay (ABI Prism SNaPshot, Fig 5B). First, RT-PCR products spanning *MLH1* exons 8 to 12 were obtained, as described above, from a peripheral blood RNA sample of a patient carrying the heterozygous c.793C>T substitution in *MLH1* exon 10 (Patient P_{793CT.1}). In parallel, a segment encompassing *MLH1* exon 10 was amplified by PCR from the genomic DNA of the same patient by using the Multiplex PCR kit (Qiagen) according to the manufacturer's instructions. Briefly, PCR reactions (35 cycles of amplification) were performed in a final volume of 25 µl with 100 ng of genomic DNA as template, a forward primer in *MLH1* intron 9 (MLH1-10-Bam-F, 5'-GACCGGATCCTTGGAAAGTGGCGACAGG-3') and a reverse primer in intron 10 (MLH1-10-Mlu-R, 5'-GACCACGCGTAATTAGTGAATAAATGAAGGAAAA-3'). Then, 5 µl aliquots of RT-PCR and PCR products were treated with one unit of Shrimp Alkaline Phosphatase (SAP, USB) and 8 units of Exonuclease I (Thermo Scientific) in the presence of SAP buffer in a final volume of 10 µl. After 1 hour at 37°C, the reactions were terminated by incubating at 75°C for 15 minutes. Next, 2 µl aliquots of treated RT-PCR and PCR products were subjected to SNaPshot reactions, in a final volume of 10 µl, by using the SNaPshot Multiplex Kit (Applied Biosystems) and a reverse primer targeting the sequence immediately downstream *MLH1* c.793C>T (SNAP-M1.793-R, 5'-GGAAGTTGATTCTACCAGAC-3'). SNaPshot reactions were carried out by performing 25 cycles of primer extension (denaturation at 96°C for 10 sec, annealing at 50°C for 5 sec and elongation at 60°C for 30 sec). Next, the reactions were incubated with 1 unit of SAP at 37°C for 1 hour, and terminated at 75°C for 15 minutes. Finally, the extension products were separated by electrophoresis and analyzed quantitatively by using an ABI PRISM-3100 Genetic Analyzer (Applied Biosystems). SNaPshot results obtained from patient cDNA were normalized by those obtained from gDNA.

Supporting Information

S1 Fig. Description of the RT-PCR products obtained in the pSPL3m-M1e10 minigene splicing reporter assay. (A) Comparative RT-PCR analysis of the splicing patterns of wild-type and mutant pSPL3m-M1e10 minigenes, as indicated. The image shows the RT-PCR products separated on a 2.5% agarose gel as described in Fig 1C. (B) Splicing events underlying the production of the major (a, b and c) and minor (d, e and f) RT-PCR products visualized in (A). As indicated, RT-PCR products were separated into 3 groups according to the splicing behavior of *MLH1* exon 10. Boxes represent exons and lines in between indicate introns. c3'ss and c5'ss indicate the positions of activated intronic cryptic 3' and 5' splice sites, respectively, whereas n5'ss refers to the creation of a new 5'ss internal to exon 10. Dotted boxes represent pseudoexons (pEx), and numbers in brackets indicate the size of the RT-PCR products. (C) *In silico* predictions relative to the strength of the 5'splice sites (new 5'ss and reference 5'ss) described in (B). *In silico* analysis was performed for wild-type (WT), and *MLH1* variants c.840T>A and c.842C>T, by using three different algorithms (SSF, MES and HSF), as indicated. The coordinates of the last exonic position of each exon/intron junction defined by the aforementioned 5' splice sites are indicated between brackets. SSF, SpliceSiteFinder-like; MES, MaxEntScan and HSF-ss, Human Splicing Finder- splice site dedicated. (TIF)

S2 Fig. Characterization of exon 10 skipping mutations by using a pCAS2-M1e10 minigene splicing reporter assay. (A) Structure of the minigenes used in the pCAS2-M1e10 splicing reporter assay. Boxes represent exons and lines in between indicate introns. The minigenes were generated by inserting a genomic fragment containing *MLH1* exon 10 and flanking intronic

sequences (*MLH1* c.791-168_c.884+187) into the intron of pCAS2, as described under Materials and Methods. Arrows above the exons represent RT-PCR primers used in the splicing reporter assay. CMV, CMV promoter; Poly A, polyadenylation site. (B) Analysis of the splicing pattern of pCAS2-M1e10 minigenes. Wild-type (WT) and mutant pCAS2-M1e10 constructs were transfected into HeLa cells and then the minigenes' transcripts were analyzed by RT-PCR as described under Materials and Methods. The top panel shows the RT-PCR products separated on a 2.5% agarose gel stained with ethidium bromide. The identities of the two major RT-PCR products, with or without exon 10 (a and b, respectively), are indicated on the left. The additional product c corresponds to exon 10 deleted of the last 48 nucleotides (splicing event explained in [S1 Fig](#) for product f). Product d is described in (C). The bottom panel shows the quantification of the RT-PCR products. Results are shown as the average of three independent experiments and are expressed as percentage of exon inclusion. Error bars indicate individual standard deviation (SD) values, whereas the horizontal dashed line delineates the lower limit of the SD bar observed for WT (93 ± 2 ; i.e. 91% lower limit of exon inclusion). Variants producing exon inclusion levels under this value were considered as exon-skipping mutations. (C) Splicing events underlying the production of the RT-PCR product d visualized in (B). c5'ss indicates the position of an intronic cryptic 5' splice site activated in the presence of *MLH1* variants located at c.883 and c.884. The dotted box represents the resulting 150 nt- intronic retention. (D) *In silico* predictions relative to the strength of the 5' splice sites (cryptic 5'ss and reference 5'ss) described in (C). *In silico* analysis was performed by using three different algorithms (SSF, MES and HSF), as indicated. The coordinates of the last exonic position of each exon/intron junction defined by the aforementioned 5' splice sites are indicated between brackets. SSF, SpliceSiteFinder-like; MES, MaxEntScan; and HSF-ss, Human Splicing Finder- splice site dedicated. (TIF)

S3 Fig. Splice site-dedicated bioinformatics tools can predict the impact on splicing of *MLH1* exon 10 variants. (A) Distribution of the seven *MLH1* exon 10 SNVs located within the reference 3' and 5' splice site consensus sequences (3'ss and 5'ss, respectively). The diagram shows the nucleotide composition of *MLH1* exon 10 (c.791-c.884), as well as the position and identity of each SNV. 3'ss and 5'ss indicate the position of reference exon/intron junctions. (B) Comparison of splice site-dedicated *in silico* predictions with experimental data obtained in the pSLP3m-M1e10 minigene splicing reporter assay. *In silico* analysis was performed for wild-type (WT) and the aforementioned mutants by using three different algorithms (SSF, MES and HSF-ss), as indicated. 3'ss and 5'ss refers to *MLH1* exon 10 reference 3' and 5' splice sites, respectively. SSF, SpliceSiteFinder-like; MES, MaxEntScan and HSF-ss, Human Splicing Finder- splice site dedicated; Δ, change relative to WT expressed as a percentage. The range of values is indicated into brackets for each tool. (C) Comparison of the 5'ss score change relative to WT obtained *in silico*, with exon 10 inclusion level change obtained in pSPL3m-M1e10 and pCAS2-M1e10 minigene assays for the last 6 mutations of exon 10. (TIF)

S4 Fig. Optimization of reaction conditions for semi-quantitative RT-PCR analysis of *MLH1* transcripts expressed in blood cells. (A) Preliminary RT-PCR reactions were performed with increasing number of PCR cycles in order to determine the linear range of the assay. The image shows the RT-PCR products obtained from fresh blood RNA of 3 healthy control individuals (C1, C2 and C3) and a patient carrying the heterozygous *MLH1* c.793C>T variant (P_{793CT.1}), separated on a 2% agarose gel, as described under Materials and Methods. The identity of the RT-PCR products is indicated on the right of the gel. M, size marker (100 bp DNA ladder); FL, full-length; Δ, exon skipping. (B) Splicing events underlying the production of the RT-PCR products visualized in (A). Boxes represent exons and lines in between

indicate introns. The different box shapes correspond to the phasing of each exon in terms of protein coding sequence, as illustrated in the lower right corner of the figure. Arrows above the exons symbolize the primers used in the RT-PCR reactions. The expected *MLH1* RNA (r.) and protein (p.) species are indicated on the right. Transcripts carrying a PTC are considered potential targets for nonsense-mediated decay (NMD). PTC, premature termination codon; FL, full-length; Δ , exon skipping.

(TIF)

S5 Fig. Comparison of pCAS2-BRCA2 exon 7 minigene data [17] with results obtained from new ESR-dedicated bioinformatics tools. Top, middle and bottom panels refer to results obtained with Δ tESRseq-, Δ HZ_{EL}- and $\Delta\Psi$ -based bioinformatics approaches, respectively, as described under Materials and Methods. *BRCA2* exon 7 variants located within the sequences that define the reference splice sites were eliminated from this analysis. Retained variants were separated into 2 groups depending on their impact on splicing as determined on the pCAS2-B2e7 minigene assay [17] and indicated above the graphs. P-values were calculated by using the Student's t-test as described under Materials and Methods. Horizontal dashes delineate the upper thresholds.

(TIF)

S6 Fig. Correlation analysis between *BRCA2* exon 7 inclusion levels [17] and results obtained from new ESR-dedicated bioinformatics tools. (A), (B) and (C) refer to results obtained with Δ tESRseq-, Δ HZ_{EL}- and $\Delta\Psi$ -based bioinformatics approaches, respectively, as described under Materials and Methods. Only *BRCA2* exon 7 variants located outside the sequences that define the reference splice sites were retained for this analysis as already mentioned in S5 Fig. The precise correspondence between each Δ value (Δ tESRseq, Δ HZ_{EL} or $\Delta\Psi$), the level of exon inclusion observed in the pCAS2-B2e7 minigene assays [17], and the identity of the corresponding *BRCA2* exon 7 variant, is indicated on S2 Table. Correlation coefficients (ρ) and p-values were determined by performing a Pearson correlation analysis, as described under Materials and Methods.

(TIF)

S7 Fig. Detection of aberrant splicing in a patient carrying the heterozygous *MLH1* c.842C>T variant. (A) Relative position of *MLH1* SNVs detected in patients P_{791-5TG.1} (c.791-5T>G), P_{842CT.1} (c.842C>T) and P_{882CT.1} (c.882C>T). Boxes represent exons and lines in between indicate introns. The different box shapes correspond to the phasing of each exon in terms of protein coding sequence, as described in S4 Fig. Arrows above the exons represent primers used in RT-PCR reactions. (B) Comparative RT-PCR analysis of RNA samples obtained from puromycin-untreated and puromycin-treated LCLs (-Puro and +Puro, respectively) derived from 3 healthy control individuals (T401, T403 and T404) and patients carrying the heterozygous variants *MLH1* c.791-5T>G (P_{791-5TG.1}), c.842C>T (P_{842CT.1}) and c.882C>T (P_{882CT.1}). RT-PCR reactions were performed with primers mapping to *MLH1* exon 8 (forward primer) and exon 12 (reverse primer), as described under Materials and Methods. The figure shows the RT-PCR products separated on a 2% agarose gel. RT-PCR product identifiers are indicated on the right of the gel. FL, full-length; Δ , exon skipping. (C) Assessment of *MLH1* allelic expression in patients P_{791-5TG.1} (c.791-5T>G), P_{842CT.1} (c.842C>T) and P_{882CT.1} (c.882C>T) by gDNA and cDNA sequencing, as indicated. Sequencing of gDNA and cDNA from T401, T403 and T404 (healthy controls described above) showed the absence of SNVs in *MLH1* exon 10 and the presence of homozygous SNP in exon 8 (T401 and T404, *MLH1* c.655AA; and T403, *MLH1* c.655GG). SNP Ex8, rs1799977 (*MLH1* c.655A>G, p.Ile219Val).

(TIF)

S1 Table. Comparison of pSPL3m-M1e10 minigene data with bioinformatics predictions based on Δ tESRseq, Δ HZ_{EI} and $\Delta\Psi$ values.

(DOCX)

S2 Table. Comparison of minigene splicing data with ESR-dedicated bioinformatics predictions for *MLH1* exon 10 variants.

(DOC)

S3 Table. Comparison of minigene splicing data with ESR-dedicated bioinformatics predictions for *BRCA2* exon 7 variants.

(DOC)

S4 Table. Comparison of minigene splicing data with ESR-dedicated bioinformatics predictions for *BRCA1* exon 6 variants.

(DOC)

S5 Table. Comparison of minigene splicing data with ESR-dedicated bioinformatics predictions for *CFTR* exon 12 variants.

(DOC)

S6 Table. Comparison of minigene splicing data with ESR-dedicated bioinformatics predictions for *NF1* exon 37 variants.

(DOC)

S7 Table. Comparative statistical analysis of the predictive power of four ESR-dedicated bioinformatics approaches by using five independent datasets.

(DOC)

S8 Table. Comparative analysis of the sensitivity and specificity of ESR-dedicated bioinformatics approaches in predicting exon-skipping mutations by using five independent datasets.

(DOC)

S9 Table. Explanations for the exceptions in the total number of variants taken into account in statistical analyses described in [S3](#), [S7](#) and [S8](#) Tables.

(DOC)

Acknowledgments

We thank the members of our Research Unit (Inserm UMR 1079, Rouen) for their input, in particular Christiane Duponchel and Françoise Charbonnier for technical assistance in preparing the pCAS2 construct and in allele-specific expression experiments, respectively, as well as Camille Charbonnier for helping with statistical analysis. We are also grateful to Jacques Bénichou (Inserm U657, University Hospital of Rouen) for a helpful discussion on statistical issues. Moreover, we thank Marine Guillaud-Bataille (Institut Gustave-Roussy, Villejuif) and Marie-Pierre Buisine (University Hospital of Lille) for generously providing lymphoblastoid cell lines from patients carrying *MLH1* SNVs c.842C>T, and c.791-5T>G and c.882C>T, respectively.

Author Contributions

Conceived and designed the experiments: OS AM. Performed the experiments: OS MH AD. Analyzed the data: OS. Contributed reagents/materials/analysis tools: PG SBD TF MT. Wrote the paper: OS AM PG.

References

1. Rabbani B, Tekin M, Mahdih N. The promise of whole-exome sequencing in medical genetics. *J Hum Genet.* 2014; 59: 5–15. doi: [10.1038/jhg.2013.114](https://doi.org/10.1038/jhg.2013.114) PMID: [24196381](https://pubmed.ncbi.nlm.nih.gov/24196381/)
2. Frebourg T. The challenge for the next generation of medical geneticists. *Hum Mutat.* 2014; 35: 909–911. doi: [10.1002/humu.22592](https://doi.org/10.1002/humu.22592) PMID: [24838402](https://pubmed.ncbi.nlm.nih.gov/24838402/)
3. Wu J, Li Y, Jiang R. Integrating multiple genomic data to predict disease-causing nonsynonymous single nucleotide variants in exome sequencing studies. *PLoS Genet.* 2014; 10: e1004237. doi: [10.1371/journal.pgen.1004237](https://doi.org/10.1371/journal.pgen.1004237) PMID: [24651380](https://pubmed.ncbi.nlm.nih.gov/24651380/)
4. Pabinger S, Dander A, Fischer M, Snajder R, Sperk M, Efremova M, et al. A survey of tools for variant analysis of next-generation genome sequencing data. *Brief Bioinform.* 2014; 15: 256–278. doi: [10.1093/bib/bbs086](https://doi.org/10.1093/bib/bbs086) PMID: [23341494](https://pubmed.ncbi.nlm.nih.gov/23341494/)
5. Eggington JM, Bowles KR, Moyes K, Manley S, Esterling L, Sizemore S, et al. A comprehensive laboratory-based program for classification of variants of uncertain significance in hereditary cancer genes. *Clin Genet.* 2014; 86: 229–237. doi: [10.1111/cge.12315](https://doi.org/10.1111/cge.12315) PMID: [24304220](https://pubmed.ncbi.nlm.nih.gov/24304220/)
6. Kichaev G, Yang W-Y, Lindstrom S, Hormozdiari F, Eskin E, Price AL, et al. Integrating functional data to prioritize causal variants in statistical fine-mapping studies. *PLoS Genet.* 2014; 10: e1004722. doi: [10.1371/journal.pgen.1004722](https://doi.org/10.1371/journal.pgen.1004722) PMID: [25357204](https://pubmed.ncbi.nlm.nih.gov/25357204/)
7. González-Pérez A, López-Bigas N. Improving the assessment of the outcome of nonsynonymous SNVs with a consensus deleteriousness score, Condel. *Am J Hum Genet.* 2011; 88: 440–449. doi: [10.1016/j.ajhg.2011.03.004](https://doi.org/10.1016/j.ajhg.2011.03.004) PMID: [21457909](https://pubmed.ncbi.nlm.nih.gov/21457909/)
8. Cline MS, Karchin R. Using bioinformatics to predict the functional impact of SNVs. *Bioinforma Oxf Engl.* 2011; 27: 441–448.
9. Frousios K, Iliopoulos CS, Schlitt T, Simpson MA. Predicting the functional consequences of non-synonymous DNA sequence variants—evaluation of bioinformatics tools and development of a consensus strategy. *Genomics.* 2013; 102: 223–228. doi: [10.1016/j.ygeno.2013.06.005](https://doi.org/10.1016/j.ygeno.2013.06.005) PMID: [23831115](https://pubmed.ncbi.nlm.nih.gov/23831115/)
10. Cartegni L, Chew SL, Krainer AR. Listening to silence and understanding nonsense: exonic mutations that affect splicing. *Nat Rev Genet.* 2002; 3: 285–298. PMID: [11967553](https://pubmed.ncbi.nlm.nih.gov/11967553/)
11. Sterne-Weiler T, Howard J, Mort M, Cooper DN, Sanford JR. Loss of exon identity is a common mechanism of human inherited disease. *Genome Res.* 2011; 21: 1563–1571. doi: [10.1101/gr.118638.110](https://doi.org/10.1101/gr.118638.110) PMID: [21750108](https://pubmed.ncbi.nlm.nih.gov/21750108/)
12. Spurdle AB, Couch FJ, Hogervorst FBL, Radice P, Sinilnikova OM. Prediction and Assessment of Splicing Alterations: Implications for clinical testing. *Hum Mutat.* 2008; 29: 1304–1313. doi: [10.1002/humu.20901](https://doi.org/10.1002/humu.20901) PMID: [18951448](https://pubmed.ncbi.nlm.nih.gov/18951448/)
13. Tournier I, Vezain M, Martins A, Charbonnier F, Baert-Desurmont S, Olschwang S, et al. A large fraction of unclassified variants of the mismatch repair genes MLH1 and MSH2 is associated with splicing defects. *Hum Mutat.* 2008; 29: 1412–1424. doi: [10.1002/humu.20796](https://doi.org/10.1002/humu.20796) PMID: [18561205](https://pubmed.ncbi.nlm.nih.gov/18561205/)
14. Théry JC, Krieger S, Gaildrat P, Révillion F, Buisine M-P, Killian A, et al. Contribution of bioinformatics predictions and functional splicing assays to the interpretation of unclassified variants of the BRCA genes. *Eur J Hum Genet EJHG.* 2011; 19: 1052–1058. doi: [10.1038/ejhg.2011.100](https://doi.org/10.1038/ejhg.2011.100) PMID: [21673748](https://pubmed.ncbi.nlm.nih.gov/21673748/)
15. Houdayer C, Caux-Moncoutier V, Krieger S, Barrois M, Bonnet F, Bourdon V, et al. Guidelines for splicing analysis in molecular diagnosis derived from a set of 327 combined in silico/in vitro studies on BRCA1 and BRCA2 variants. *Hum Mutat.* 2012; 33: 1228–1238. doi: [10.1002/humu.22101](https://doi.org/10.1002/humu.22101) PMID: [22505045](https://pubmed.ncbi.nlm.nih.gov/22505045/)
16. Ke S, Shang S, Kalachikov SM, Morozova I, Yu L, Russo JJ, et al. Quantitative evaluation of all hexamers as exonic splicing elements. *Genome Res.* 2011; 21: 1360–1374. doi: [10.1101/gr.119628.110](https://doi.org/10.1101/gr.119628.110) PMID: [21659425](https://pubmed.ncbi.nlm.nih.gov/21659425/)
17. Di Giacomo D, Gaildrat P, Abuli A, Abdat J, Frébourg T, Tosi M, et al. Functional analysis of a large set of BRCA2 exon 7 variants highlights the predictive value of hexamer scores in detecting alterations of exonic splicing regulatory elements. *Hum Mutat.* 2013; 34: 1547–1557. doi: [10.1002/humu.22428](https://doi.org/10.1002/humu.22428) PMID: [23983145](https://pubmed.ncbi.nlm.nih.gov/23983145/)
18. Erkelenz S, Theiss S, Otte M, Wiedera M, Peter JO, Schaal H. Genomic HEXploring allows landscaping of novel potential splicing regulatory elements. *Nucleic Acids Res.* 2014; 42: 10681–10697. doi: [10.1093/nar/gku736](https://doi.org/10.1093/nar/gku736) PMID: [25147205](https://pubmed.ncbi.nlm.nih.gov/25147205/)
19. Xiong HY, Alipanahi B, Lee LJ, Bretschneider H, Merico D, Yuen RKC, et al. The human splicing code reveals new insights into the genetic determinants of disease. *Science.* 2014;
20. Baralle D, Lucassen A, Buratti E. Missed threads. The impact of pre-mRNA splicing defects on clinical practice. *EMBO Rep.* 2009; 10: 810–816. doi: [10.1038/embor.2009.170](https://doi.org/10.1038/embor.2009.170) PMID: [19648957](https://pubmed.ncbi.nlm.nih.gov/19648957/)

21. Lim KH, Ferraris L, Filloux ME, Raphael BJ, Fairbrother WG. Using positional distribution to identify splicing elements and predict pre-mRNA processing defects in human genes. *Proc Natl Acad Sci U S A*. 2011; 108: 11093–11098. doi: [10.1073/pnas.1101135108](https://doi.org/10.1073/pnas.1101135108) PMID: [21685335](https://pubmed.ncbi.nlm.nih.gov/21685335/)
22. Grandval P, Fabre AJ, Gaildrat P, Baert-Desurmont S, Buisine M-P, Ferrari A, et al. UMD-MLH1/MSH2/MSH6 databases: description and analysis of genetic variations in French Lynch syndrome families. *Database J Biol Databases Curation*. 2013; 2013: bat036.
23. Thompson BA, Spurdle AB, Plazzer J-P, Greenblatt MS, Akagi K, Al-Mulla F, et al. Application of a 5-tiered scheme for standardized classification of 2,360 unique mismatch repair gene variants in the InSiGHT locus-specific database. *Nat Genet*. 2014; 46: 107–115. doi: [10.1038/ng.2854](https://doi.org/10.1038/ng.2854) PMID: [24362816](https://pubmed.ncbi.nlm.nih.gov/24362816/)
24. Lastella P, Surdo NC, Resta N, Guanti G, Stella A. In silico and in vivo splicing analysis of MLH1 and MSH2 missense mutations shows exon- and tissue-specific effects. *BMC Genomics*. 2006; 7: 243. PMID: [16995940](https://pubmed.ncbi.nlm.nih.gov/16995940/)
25. Charbonnier F, Martin C, Scotte M, Sibert L, Moreau V, Frebourg T. Alternative splicing of MLH1 messenger RNA in human normal cells. *Cancer Res*. 1995; 55: 1839–1841. PMID: [7728749](https://pubmed.ncbi.nlm.nih.gov/7728749/)
26. Genuardi M, Viel A, Bonora D, Capozzi E, Bellacosa A, Leonardi F, et al. Characterization of MLH1 and MSH2 alternative splicing and its relevance to molecular testing of colorectal cancer susceptibility. *Hum Genet*. 1998; 102: 15–20. PMID: [9490293](https://pubmed.ncbi.nlm.nih.gov/9490293/)
27. Thompson BA, Martins A, Spurdle AB. A review of mismatch repair gene transcripts: issues for interpretation of mRNA splicing assays. *Clin Genet*. 2014.
28. Vezain M, Saugier-Verber P, Goina E, Touraine R, Manel V, Toutain A, et al. A rare SMN2 variant in a previously unrecognized composite splicing regulatory element induces exon 7 inclusion and reduces the clinical severity of spinal muscular atrophy. *Hum Mutat*. 2010; 31: E1110–1125. doi: [10.1002/humu.21173](https://doi.org/10.1002/humu.21173) PMID: [19953646](https://pubmed.ncbi.nlm.nih.gov/19953646/)
29. Raponi M, Kralovicova J, Copson E, Divina P, Eccles D, Johnson P, et al. Prediction of single-nucleotide substitutions that result in exon skipping: identification of a splicing silencer in BRCA1 exon 6. *Hum Mutat*. 2011; 32: 436–444. doi: [10.1002/humu.21458](https://doi.org/10.1002/humu.21458) PMID: [21309043](https://pubmed.ncbi.nlm.nih.gov/21309043/)
30. Cartegni L, Wang J, Zhu Z, Zhang MQ, Krainer AR. ESEfinder: A web resource to identify exonic splicing enhancers. *Nucleic Acids Res*. 2003; 31: 3568–3571. PMID: [12824367](https://pubmed.ncbi.nlm.nih.gov/12824367/)
31. Smith PJ, Zhang C, Wang J, Chew SL, Zhang MQ, Krainer AR. An increased specificity score matrix for the prediction of SF2/ASF-specific exonic splicing enhancers. *Hum Mol Genet*. 2006; 15: 2490–2508. PMID: [16825284](https://pubmed.ncbi.nlm.nih.gov/16825284/)
32. Desmet F-O, Hamroun D, Lalande M, Collod-Bérout G, Claustres M, Bérout C. Human Splicing Finder: an online bioinformatics tool to predict splicing signals. *Nucleic Acids Res*. 2009; 37: e67. doi: [10.1093/nar/gkp215](https://doi.org/10.1093/nar/gkp215) PMID: [19339519](https://pubmed.ncbi.nlm.nih.gov/19339519/)
33. Pagani F, Stuaní C, Tzetis M, Kanavakis E, Efthymiadou A, Doudounakis S, et al. New type of disease causing mutations: the example of the composite exonic regulatory elements of splicing in CFTR exon 12. *Hum Mol Genet*. 2003; 12: 1111–1120. PMID: [12719375](https://pubmed.ncbi.nlm.nih.gov/12719375/)
34. Pagani F, Raponi M, Baralle FE. Synonymous mutations in CFTR exon 12 affect splicing and are not neutral in evolution. *Proc Natl Acad Sci U S A*. 2005; 102: 6368–6372. PMID: [15840711](https://pubmed.ncbi.nlm.nih.gov/15840711/)
35. Baralle M, Skoko N, Knezevich A, De Conti L, Motti D, Bhuvanagiri M, et al. NF1 mRNA biogenesis: effect of the genomic milieu in splicing regulation of the NF1 exon 37 region. *FEBS Lett*. 2006; 580: 4449–4456. PMID: [16870183](https://pubmed.ncbi.nlm.nih.gov/16870183/)
36. Auclair J, Busine MP, Navarro C, Ruano E, Montmain G, Desseigne F, et al. Systematic mRNA analysis for the effect of MLH1 and MSH2 missense and silent mutations on aberrant splicing. *Hum Mutat*. 2006; 27: 145–154. PMID: [16395668](https://pubmed.ncbi.nlm.nih.gov/16395668/)
37. Gaildrat P, Krieger S, Di Giacomo D, Abdat J, Révillion F, Caputo S, et al. Multiple sequence variants of BRCA2 exon 7 alter splicing regulation. *J Med Genet*. 2012; 49: 609–617. doi: [10.1136/jmedgenet-2012-100965](https://doi.org/10.1136/jmedgenet-2012-100965) PMID: [22962691](https://pubmed.ncbi.nlm.nih.gov/22962691/)
38. Prior TW, Krainer AR, Hua Y, Swoboda KJ, Snyder PC, Bridgeman SJ, et al. A positive modifier of spinal muscular atrophy in the SMN2 gene. *Am J Hum Genet*. 2009; 85: 408–413. doi: [10.1016/j.ajhg.2009.08.002](https://doi.org/10.1016/j.ajhg.2009.08.002) PMID: [19716110](https://pubmed.ncbi.nlm.nih.gov/19716110/)
39. Liu F, Gong C-X. Tau exon 10 alternative splicing and tauopathies. *Mol Neurodegener*. 2008; 3: 8. doi: [10.1186/1750-1326-3-8](https://doi.org/10.1186/1750-1326-3-8) PMID: [18616804](https://pubmed.ncbi.nlm.nih.gov/18616804/)
40. Plotz G, Raedle J, Brieger A, Trojan J, Zeuzem S. N-terminus of hMLH1 confers interaction of hMutLalpha and hMutLbeta with hMutSalph. *Nucleic Acids Res*. 2003; 31: 3217–3226. PMID: [12799449](https://pubmed.ncbi.nlm.nih.gov/12799449/)
41. Buckler AJ, Chang DD, Graw SL, Brook JD, Haber DA, Sharp PA, et al. Exon amplification: a strategy to isolate mammalian genes based on RNA splicing. *Proc Natl Acad Sci U S A*. 1991; 88: 4005–4009. PMID: [1850845](https://pubmed.ncbi.nlm.nih.gov/1850845/)

42. Gaildrat P, Killian A, Martins A, Tournier I, Frébourg T, Tosi M. Use of splicing reporter minigene assay to evaluate the effect on splicing of unclassified genetic variants. *Methods Mol Biol Clifton NJ*. 2010; 653: 249–257.
43. Ho SN, Hunt HD, Horton RM, Pullen JK, Pease LR. Site-directed mutagenesis by overlap extension using the polymerase chain reaction. *Gene*. 1989; 77: 51–59. PMID: [2744487](#)